DESIGN AND DEVELOPMENT OF THE D8 COMMERCIAL TRANSPORT CONCEPT

Brian Yutko, Neil Titchener, Christopher Courtin, Michael Lieu, Larry Wirsing, David Hall, John Tylko, Jeffrey Chambers, Thomas Roberts, Clint Church

Aurora Flight Sciences, A Boeing Company

Abstract

The conceptual design of a subsonic, environmentally efficient, twin-aisle commercial airliner is presented (previously presented by Yutko et al [1]). The D8 double-bubble aircraft – named for its complex, non-round fuselage shape – originated from NASA's N+3 Phase I study in which participants designed efficient commercial aircraft for market entry in the 2035 timeframe. Previous computational and experimental work has established the potential of the D8 configuration to significantly reduce environmental impact of aviation. However, the integration of engines and airframe, as well as the non-round fuselage with central support element, pose many challenges for the airframe designer. In this paper, the conceptual design of a D8 aircraft is presented: the aircraft is designed to comply with FAR 25 requirements and air transportation system constraints; airframe structural solutions for the unique configuration challenges of the D8 are presented; aircraft weight and balance and airline operations are analyzed; aerodynamic lofting and performance is accomplished with CFD; and performance of the boundary layer ingesting (BLI) propulsion system is investigated. Results are presented for two D8 concepts. First, a concept for a D8 with an entry-into-service (EIS) of 2016 was designed that utilizes current engine technology and existing composite manufacturing techniques, and it is demonstrated that such an aircraft is capable of saving between 25-30% fuel when compared with a Boeing 737-800. Second, a concept for a vision system with EIS prior to 2035 that is capable of meeting NASA's mid-term environmental goals was designed. An air transportation system analysis was completed using these aircraft and it is shown that the D8 configuration has the potential to reduce narrowbody system fuel consumption by 52% and significantly reduce community noise impacts based on an analysis of the top 20 United States airports.

1 Introduction and Aircraft Configuration Background

Over the past eighty years of commercial airline operations, only two fundamental transitions in aircraft configuration occurred. In both cases, government funding supplemented by private capital formed the basis for successful product launches. In recent years, similar collaboration of government and industry, with key university partners, has resulted in a series of new aircraft configurations which have the potential to again revolutionize commercial airline economics with significant operating benefits related to substantially reduced fuel burn and much smaller environmental impact.

The first revolution was the launch of the DC-3 by Douglas Aircraft in 1935, which incorporated several new aeronautical technologies including radial air-cooled engines with cowlings, a variable pitch propeller, high-lift flaps, lightweight stressed-skin structure and retractable landing gear. NASA's predecessor, the National Advisory Committee for Aeronautics, developed several of these technologies, including the one of the first uses of a standard NACA airfoil. The Collier Trophy was awarded on three separate occasions for the government and industry innovations embodied in the DC-3: to NACA for the engine cowling with improved aerodynamic efficiency in 1929;

to Hamilton Standard for the variable pitch propeller in 1933 and to Douglas Aircraft for the DC-3 aircraft itself in 1935 [2].

The DC-3 was the first commercial airliner that could be flown by airlines at a profit. As William Littlewood, chief engineer of American Airlines would later write, the DC-3 was "the first American transport to show a favorable net difference between costs and revenues at reasonable load factors and for a substantial spread of operating ranges" [3]. By the end of the decade, DC-3 aircraft carried 95% of all US commercial air traffic and were used by 30 foreign airlines. By launching a disruptive technology, Douglas emerged as the leading commercial airliner manufacturer, a position it would maintain for nearly four decades.

In the late 1950s, the second revolution, a transition from propeller driven aircraft to jet aircraft, was also achieved through major public and private investments. In this case, the market disrupter was Boeing, which began the decade in fifth place in commercial aircraft behind Douglas, Lockheed, Martin, and Convair. Leveraging Boeing's experience with B-47 and B-52 military bombers, newly elected Boeing President William Allen made the decision to invest $16 million, a major portion of Boeing's existing financial resources, to develop a prototype aircraft, the 367-80, for both the KC-135A Stratotanker for the military and the Boeing 707 Stratoliner for commercial customers. Within a month of its first flight, Air Force General Curtis LeMay authorized an initial order of 29 KC-135A aircraft in August 1954. Boeing leveraged Air Force funding to mature the aircraft for civil aviation. Pan American World Airways placed its launch order for 20 Boeing 707 airliners in October 1956, beginning the modern jet era which Boeing Commercial Aircraft would dominate.

Exhibiting many of the fundamental characteristics described by Clay Christensen, the commercial airline industry has not adopted a new aircraft configuration in over sixty years [4]. Although aircraft fuel efficiency has steadily improved, these advances have been accomplished primarily through dramatic improvements in propulsion systems rather than substantial changes in airframe configuration. For example, the silhouettes of tube-and-wing aircraft over the past sixty years demonstrate considerable similarity [5]. Engine configurations, on the other hand, have changed from turbojets, to turbofans, to high bypass ratio turbofans, to the geared turbofans recently introduced into service [6]. Unfortunately, continuation of the current design practices will result in increased nacelle drag, increased propulsor weight, and under-wing installation challenges due to larger fans. The increasingly diminishing returns available from advances in tube-and-wing aircraft is shown in Figure 1, which shows the historical trend of fuel-burn per seat-km from the Boeing 707 through to the Boeing 737-MAX8.

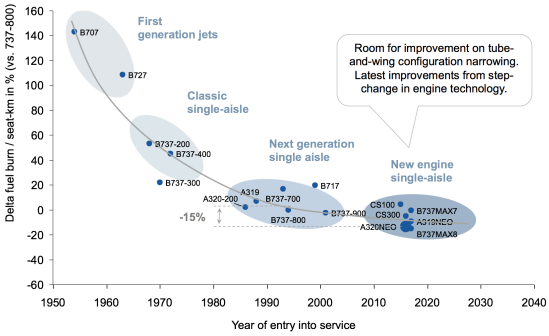

Fig. 1. Progression of fuel-burn per seat-km over time

Under the leadership of NASA Aeronautics, beginning with the N+3 program in 2008, new teams of government, industry and academic innovators aggressively pursued the systematic examination of new airframe architectures with potential for major improvements in vehicle system-level performance that go well beyond what is achievable through component or subsystem advances. Such configurations have been estimated to achieve fuel savings of up to 70 percent, compared to current versions of conventional commercial airliners.

These innovative teams primarily focused on new aircraft configurations capable of significant performance increases utilizing a high degree of integration between the propulsion system and the airframe. This level of airframe propulsion integration leads to substantial performance and efficiency improvements offered by these new configurations.

Three primary criteria were established for the next generation of aeronautical technology

capable of transforming commercial aviation the way the DC-3 and 707 did several generations ago. These aircraft should be:

- Fully integrated to leverage the virtuous cycle of interactions between subsystems in order to deliver revolutionary performance benefits in a short time frames;
- Not dependent on high-risk technologies such as low-TRL materials or manufacturing methods; and
- Capable of being integrated seamlessly into the existing global air transportation system.

The importance of seamless integration into the global air transportation cannot be overstated. Advanced, fuel efficient concepts have existed for decades, but they have not been produced because of both commercial pressure against cannibalizing existing product lines and pushback by customers against major changes to the way aircraft are typically operated. In the same way that new jet aircraft like the 707 leveraged existing infrastructure and could be operated profitably while improving the airline customer experience, a new revolutionary aircraft based on an innovative configuration must be compliant with airport infrastructure, provide a substantial operating cost savings to airlines, and achieve passenger experiences equal to or better than today's best-in-class aircraft.

2 D8 Background and Configuration Requirements

The D8 originated from NASA's N+3 Phase I study, during which a team from the Massachusetts Institute of Technology (M.I.T), Aurora Flight Sciences (Aurora), and Pratt & Whitney (P&W) conducted conceptual trades and system optimization studies to develop a conceptual configuration of an ultra-efficient 180-passenger transport aircraft [7] [8] [9] .The goal of the NASA N+3 program was to develop a conceptual aircraft that would substantially reduce fuel consumption, noise, and emissions of commercial aircraft with a targeted entry into service in the 2035 timeframe. The D8 is characterized by a twin-aisle lifting body fuselage with integrated Boundary Layer Ingesting (BLI) propulsion. An artist's depiction of the Aurora D8 is shown in Figure 2.

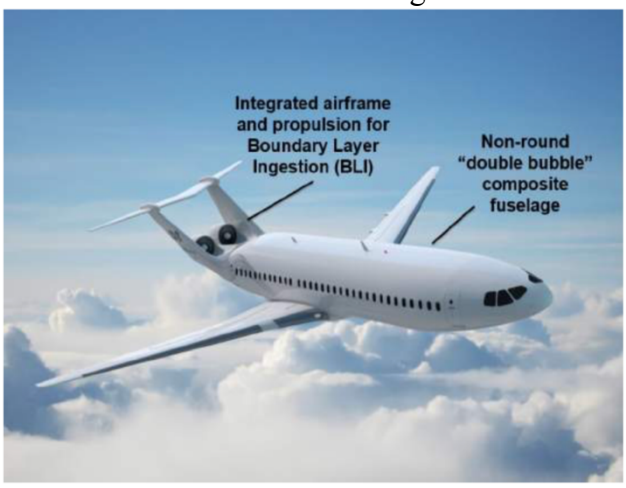

Fig. 2. Aurora D8-2016 subsonic transport aircraft

The D8 configuration's distinctive dual-lobed, double-bubble fuselage and pi-tail, greatly enhance air-vehicle performance when combined with aft-mounted boundary-layer ingestion (BLI) engines. The substantial performance benefits resulting from the D8 configuration—rather than for any of the individual technologies integrated into the aircraft—is perhaps the MIT led N+3 project's most important finding [7]. It implies that a synergistic aircraft configuration has the potential to deliver a step change in commercial aircraft performance, and that this change could potentially occur on a shorter time scale than required for maturation of many separate incremental technologies.

Motivated by the potential gains possible with the D8 configuration, researchers have continued to mature the D8 concept: Notably, de la Rosa Blanco and Hileman [8] on D8 noise performance; Pandya [11] on aerodynamic design; Hall [12] on BLI fan design; Lord et al. [13] on engine architectures suitable for the D8; and Uranga et al. [14] on an experimental assessment of the BLI benefit for the D8. In the latter research, a 1:11 scale, powered model of a D8 configuration was tested in NASA Langley's 14x22 ft. subsonic wind tunnel in order to evaluate the aerodynamic performance of the D8 with and without BLI. In this experimental investigation, a power benefit of up to 8% was directly measured validating early conceptual tool estimates.

The present work builds on these prior research programs and attempts to fill some important gaps: particularly, design of the unique structures required for the D8 aircraft, compliance with regulations and air transportation system constraints, and an updated performance assessment based on these designs. To have the largest impact on emissions, Aurora's D8 design is targeted at the largest segment of the commercial aircraft market: The single-aisle, 150-200 passenger, 3000 nm range segment currently dominated by the Boeing 737 and Airbus A320 families of aircraft. Therefore, the current study took the design point to be 180 passengers with a transcontinental range of 3000-nm. In addition, a design cruise Mach number of 0.80 was selected for ease of integration into the existing air transportation network which led to long range cruise performance occurring at approximately 0.78M. It is worth noting that this cruise Mach number is higher than the MIT Phase I D8 design which was designed to minimize fuel-burn and resulted in a 0.72M aircraft. A balanced field length constraint of 8000 ft. was also included to retain similar airfield operational capabilities as the B737-800. Aurora introduced several other design constraints/requirements beyond those included in the original MIT Phase I including a span constraint of 118 ft. The design mission shown in Figure 3 was defined prior to conceptual design to be similar to the B737-800. The design payload is 180 passengers each weighing 195 lbs. in accordance with AC120- 27E [15].

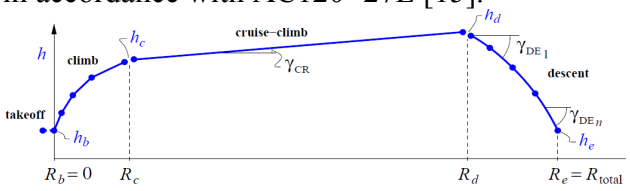

Fig. 3. Design mission with a constant cruise climb

Key features of the design mission are the 250 KIAS speed restriction under 10,000ft, and a Mach 0.78 optimal cruise climb, which would be approximated by a step climb under current ATC regulations. As part of the vehicle design process, the initial cruise altitude was a free variable that could be optimized along with other vehicle

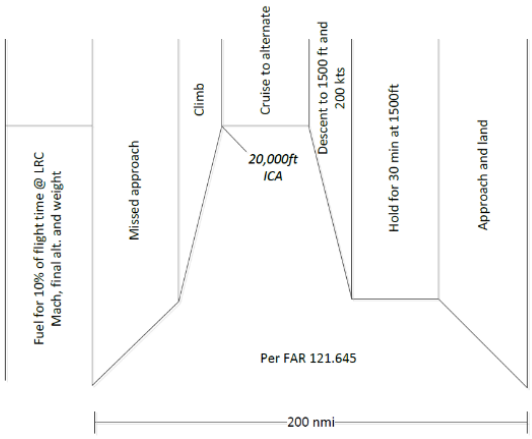

Fig. 4. Fuel reserve mission based on FAR 121.645 and ATA best practice

parameters such as wing size, fan diameter, etc. All other features of the mission were fixed.

The reserve fuel fraction was calculated based on the requirements of FAR 121.645 and the industry best practices. The mission profile for the reserve fuel is shown in Figure 4 and consists of fuel for 10% of the original mission plus a missed approach at the original destination airport, a 200-mile cruise to the alternate at 20,000ft, and a 30-minute hold at 1500 ft. before landing. The total fuel for such a reserve mission turns out to be approximately 20% for such a design payload and range.

The performance of the D8 variants described in this paper is assessed against NASA's Subsonic Transport System-level Metrics (STSLM) [16]. These metrics, which are shown in Table 1, specify near-, mid-, and far term targets for aircraft noise, fuel burn, and emissions, referenced to a common baseline. The common baseline is generally accepted to be the Boeing 737-800 powered by two CFM56-7 series engines; an all-aluminum, tube-and-wing aircraft with moderate bypass ratio engines.

Technology Benefit	Technology Generations		
	Near-term 2015-2025	Mid-term 2025-2035	Far-term Beyond 2035
Noise (cumulative below Stage 4)	22-32 dB	32-42 dB	42-52 dB
LTO NOx Emissions (below CAEP 6)	70-75%	80%	>80%
Cruise NOx Emissions (relative to 2005 best in class)	65-70%	80%	>80%
Fuel/Energy Consumption (relative to 2005 best in class)	40-50%	50-60%	60-80%

Table 1. NASA Subsonic Transport System Level Metrics for noise and fuel economy

3 Conceptual Design Method

The conceptual design of the D8 aircraft presented in this paper follows a standard iterative design process in which integrated discipline teams performed repeated high-fidelity analysis and passed results onward. This spiral of fidelity can continue onwards through preliminary design, detail design, and eventually into manufacturing as part of a product development program. As with any design study that does not end in flight or ground-test hardware, the endpoint is determined by engineering judgement—the purpose of a design study is to generate data capable of answering predetermined questions. In this case, the purpose of the design study is to generate data capable of: validating performance estimates from lower-fidelity conceptual performance tools, assessing the feasibility of the unique structures required for the D8 aircraft, evaluating the D8 against NASA vehicle-level and system-level performance metrics, and providing a point-of-departure for designing ground and flight test articles.

With any novel configuration, design integration is critical to establishing real-world design constraints and to create a practical aircraft. MIT's conceptual design tool, Transport Aircraft System OPTimization tool, TASOPT, was developed to allow optimized integrated aircraft design at the system level. As reported in "N+3 Aircraft Concept Designs and Trade Studies, Final Report" [7], TASOPT was used to define the D8 configuration and identify its fuel savings over current generation commercial transports.

Firstly, TASOPT was used for a trade-space study on various D8 aircraft. This study and the performance of the various D8 aircraft are reported in Section 4. Once the trade-studies in TASOPT were completed and a suitable seed aircraft was identified for the given constraints, the design was matured through conceptual design using higher fidelity tools and additional operational and manufacturing constraints were added. Updated D8 weight allocation, aerodynamic performance, and propulsion system performance was calculated, and the magnitude of fuel savings and aircraft noise were updated. The conceptual design of this aircraft is presented in Section 5. The 2016 technology level variant of the D8 was chosen as the seed design for the detailed design study to avoid having to include various future technologies that have unknown impacts on weight and performance.

The general design process for the full conceptual design study was conventional and followed a sequence from initial aircraft sizing to detailed geometry definition and layout. Attention was paid to passenger cabin configuration and structural layout. The steps in a single design cycle are as follows:

1. Initial sizing studies were performed with TASOPT for a Mach 0.78 LRC / 180 passenger / 3000 nm mission, with fuel reserves based on FAR Part 121.645. This determined the wing and tail areas, engine thrust, and an initial weight budget.

2. A CAD model was developed based on the TASOPT design. Main structural elements were identified, and a structural layout was developed. A layout of the passenger cabin to provide seating, baggage bins, lavatories and galleys for 180 passengers in a single-class, consistent with present day comfort levels, was generated. Both double bubble and oval cross sections were developed for a trade study of the fuselage weight.
3. A two-crew flight deck was laid out with attention paid to providing visibility consistent with current certification criteria, with and without enhanced vision systems. The effect of the cab outer mold line on the aircraft basic pitching moment was considered in an aerodynamic trade study.
4. The defining airfoils for the wing loft were chosen, and wing camber, thickness, and twist distribution were established using a vortex lattice model and compressible Euler calculations. A preliminary concept for the high lift system was selected based on similarity to current generation transports. The wing geometry planform was adjusted from the TASOPT output to provide adequate integration of the main landing gear.
5. *V-n* diagrams were generated to establish the preliminary maneuver and gust loads. The critical sizing cases were then selected.
6. A vortex lattice model was used to compute the wing, empennage and fuselage loads. The loads were the basis for initial structural sizing studies to validate the weight.
7. Horizontal and vertical tail volume coefficients were chosen. The horizontal tail size was established by setting a minimum static margin of 5% mean aerodynamic chord at the aft c.g. limit and a reasonable tail lift coefficient on approach at the forward c.g. limit. Vertical tail volume was based on similarity to current twin-engine transports.
8. Concepts for the aircraft systems were chosen and used to estimate system weights.
9. A drag buildup was generated from a combination of handbook methods based on wetted areas, induced and trim drag from a vortex lattice model, and wing drag based on two-dimensional airfoil viscous computations and sweep theory. The drag buildup was used in for detailed performance calculations.
10. A boundary-layer ingestion compliant variant of current best-in-service jet-engines was generated using an in-house variant of the TASOPT engine model which implements BLI via a power balance methodology.

Ideally, several design cycles would have been performed to close on an optimum configuration. However, this was not possible due to schedule constraints and because an optimized aircraft was not an objective of this design study. Therefore, the D8 aircraft described in this paper is *not* an optimal solution. There remain opportunities to further improve the efficiency of the aircraft – perhaps substantially – through further design cycles; those will be noted where they have been identified.

4 D8 Configuration Analysis Using TASOPT

TASOPT was created to examine and evaluate future aircraft with potentially unprecedented airframe, aerodynamic, engine, or operation parameters. For such configurations, it is desirable to dispense with as many of the historically-based methods as possible, since these cannot be relied on outside of their data-fit ranges. It is preferential instead to rely on low-order physical models implementing fundamental structural, aerodynamic, and thermodynamic theory and associated computational methods for all primary predictions. Modeling the bulk of the aircraft structure, aerodynamics, and propulsion by fundamentals gives considerable confidence that the resulting optimized design is realizable, and not some artifact of inappropriate extrapolated data fits. From Drela [8]: *TASOPT uses structural theory for primary-structure sizing and weight prediction (in lieu of historical correlations), variable wing airfoils and viscous/inviscid CFD for all profile drag prediction (in lieu of wetted-area methods), full engine flowpath simulation (in lieu of engine tables or correlations), and a variable flight trajectory (in lieu of a fixed climb and cruise*

profile). The minimal reliance on historical data and empiricism gives considerable confidence in applying TASOPT for the conceptual design of the unconventional D8 configuration.

Based on the prescribed mission and payload described in Section 2, TASOPT was utilized to perform low fidelity system-level analysis and trades on numerous variants of the D8 with various assumed technology levels. A conceptual design tool such as TASOPT is ideal for directly comparing numerous D8 variants within a common framework. The performance assessment performed as part of this study focused on the fuel-burn performance of the various D8 configurations, and the objective function optimized in TASOPT for this study was Payload Fuel Energy Intensity (PFEI), which is the fuel energy consumption per payload-range. TASOPT version 2.16 was utilized in this study which includes relatively minor updates to the engine model when compared to the original TASOPT version used in the NASA/MIT Phase I study [7].

While fuel-burn was the objective for optimization, a noise assessment of each of the D8 configurations was also undertaken relative to the baseline. The performance of each configuration with respect to NO_x emission was not specifically assessed as NO_x emissions are driven primarily by advances in core combustor technology. Given that core combustor technology is largely independent of the air vehicle geometric configuration, there was no utility in assessing NO_x performance here.

In addition to performing optimization on various D8 variants, a number of morphing sequences were performed, whereby the conceptual aircraft is discretely morphed from a known tube-and-wing configuration to various D8 configurations with varying levels of technology. These technology benefits, while not D8-specific, are an important element that is captured by the morphing approach. This methodology was employed to isolate the benefits of the D8 from various future technologies, such as advanced aerodynamics, engine technologies and composite materials, that are just as applicable to other configurations. As a result, this study identifies the unique performance benefit of the D8 relative to alternative configurations.

Before the various D8 variants were modeled, a suitable baseline tube-and-wing aircraft was established in TASOPT. This is an important step as it ensures a fair comparison is made between various conceptual-airplanes in a low-fidelity conceptual design. Using TASOPT's built-in 737-800 geometry, the performance of the TASOPT 737-800 was computed using in sizing mode (with optimization switched off). This TASOPT 737-800, differs somewhat from that in Reference [7] due to the updated engine model that better simulates engine off-takes and spool losses. The TASOPT variant of the 737-800 is presented in Table 2 alongside publicly available data for the 737-800 (without winglets) taken from the Boeing Airport Planning Guide [17]. It can be seen that very good agreement is obtained between TASOPT and published data with the OEW and block fuel for a 3000 nm mission with the design payload computed in TASOPT within 1% of published values. This result provides confidence in TASOPTs ability to produce realistic weights and block fuel performance.

The TASOPT 737-800 was then run in fuel-burn optimization mode which allows TASOPT the vary design parameters such as wing aspect

	Source		
	Boeing Airport Planning Guide	TASOPT (No Optimization)	TASOPT (Optimization)
Maximum takeoff weight (lbs)	174,000	173,790	157,053
Block fuel (lbs)	39,200*	39,458	35,409
Mission fuel weight (lbs)	47,000	47349	42,491
Operational Empty Weight (lbs)	91,300	91,346	79,467

*Assuming 20% reserve fuel

Table 2. Weight comparison of Boeing 737-800 models

ratio, cruising altitude, cruise CL, etc. The OEW, fuel-burn over the 3000 nm mission, and resulting MTOW, for the TASOPT optimized 737-800 are also shown in Table 2. From Table 2 it can be seen that there is a substantial difference between the TASOPT optimized and non-optimized 737-800. This difference stems from the fact that TASOPT creates a purely fuel-burn optimized solution; whereas, there are many other design drivers for real-world aircraft including those driven by economic and operational considerations. It is for this reason that the most meaningful comparison is that between fuel-optimized vehicles in TASOPT. The TASOPT optimized 737-800 represents a 2005 best-in-class fuel optimized, all-aluminum, tube-and-wing configuration with high-bypass engines, and, as a result, this vehicle is used as the baseline when comparing TASOPT D8 aircraft performance to the NASA fuel-burn metric.

Three D8 variants were compared to the baseline tube-and-wing as part of this study:

1. UW-D8-2016: A 2016 D8 with underwing engines: This aircraft consists of a double-bubble fuselage and pi-tail with two engines mounted conventionally under the wings. The airframe is of all-composite construction using current industry-standard composite materials, and the engines consist are geared turbofan engines representative of current state of the art designs. This is the highest TRL variant of the D8 aircraft.
2. D8-2016: A 2016 D8 with aft mounted BLI engines: This aircraft consists of the same technologies as the D8 with the addition of BLI engines. This variant is intended to demonstrate the performance benefits available using technology available today with the exception of BLI-specific engine technologies such as a distortion-tolerant fan and core designs. There is no assumption of technology advancement included in the performance numbers beyond the suitability of the engine for BLI operations.
3. D8-2035: A 2035 D8 with BLI: This aircraft includes a selection of technology packages to estimate the performance of a D8 with a 2035 entry into service (EIS). As a result, this variant includes technology advances that are expected to be matured by that timeframe, such as more advanced composites and high-temperature engine materials and ultra-high bypass ratio, small-core engine technology.

A morphing chart that illustrates one sequence of morphing from the baseline tube-and-wing configuration to the TASOPT D8-2016 is presented in Figure 5. The origin corresponds to the optimized TASOPT 737-800 as discussed above. At each step in the morphing process, as each geometric change or technology is added, the vehicle is re-optimized to minimize fuel burn over the reference mission profile. Consequently, the benefit shown at each step is the integrated vehicle-level benefit of that configuration change or technology addition and not just the direct benefit of that addition to the previous iteration. For this TASOPT study it is assumed that the TASOPT D8-2016 ingests 40% of the total fuselage surface dissipation with a 1% fan polytropic efficiency debit due to the inlet distortion

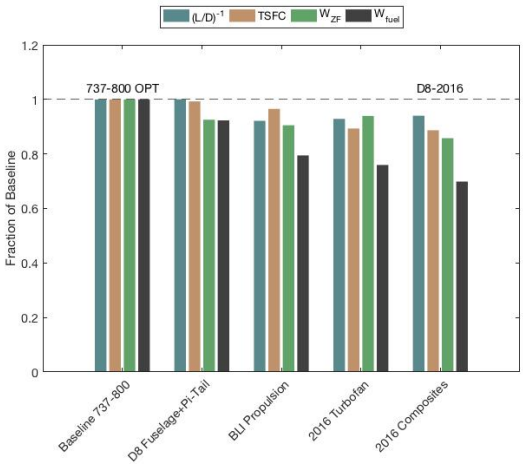

Fig. 5. Example morphing process from the TASOPT 737-800 OPT to the TASOPT D8-2016

In Figure 5, four bars are shown at each step with each step normalized by the baseline. Three of the four bars represent each of the main contributors to vehicle fuel-burn performance: lift-to-drag, L/D, which quantifies external aerodynamic efficiency, TSFC, which quantities propulsion system efficiency, and zero-fuel weight which defines structural efficiency. These are the three terms that feature in the Breguet range equation. The fourth bar shown at each step is the fuel-burn relative to the baseline aircraft. For aircraft with a relatively short

design mission, fuel-burn is almost directly proportional to these three factors which have approximately equal weighting [8]. As a result, Table 3 illustrates not only the fuel-burn benefit but also a direct breakdown of where the benefit originates as each technology or configuration change is introduced.

In reviewing the performance of the TASOPT D8-2016 it is visible that the aerodynamic, propulsion and structural performance are all improved relative to the baseline. The zero-fuel weight is improved by 14%, the propulsion system performance is improved 11% and the aerodynamic performance 6%. Consequently, there is an overall fuel-burn benefit relative to the baseline of 30%.

The benefits of the double-bubble fuselage and pi-tail in terms of air-vehicle weight is clearly shown in the first morphing step. This weight reduction is driven by the need for a smaller wing due to the lifting attributes of the fuselage and widened fuselage, and the widened fuselage and wing box reduces the root bending moment loads and hence wing box and spar weights. Furthermore, the reduced wing size precipitates a reduction in tail size and hence weight. Finally, the widened fuselage also allows landing gear can be mounted closer to the ground while retaining the required wheel base, and this reduces the total landing gear weight. While there is an improvement in lift-to-drag for the D8 configuration due to improved lift-carryover and the positive pitching moment contribution which reduces the required horizontal tail size, this is partially offset by increased wetted area of the fuselage (due to the non-cylindrical shape). As is expected, the majority of the TSFC benefit occurs at the steps in the morphing sequence where 2016 engines are introduced (7%) and with the introduction of boundary-layer ingestion (3%). The main benefit of the composites is a reduction in zero-fuel weight. The trade-off between increased engine size for improved propulsive efficiency and increased weight is also visible from the morphing chart as can be seen from the increase in zero-fuel weight with the introduction of 2016 engines.

The TASOPT optimization presented in Figure 5 has fuel-burn as the sole objective. In practice, it may be desirable to trade some fuel benefit for improvements in noise or other metrics of interest; multi-objective optimization is a compelling candidate for future work.

Figure 6 shows the results of the morphing steps in terms of both fuel-burn and noise leading to the non-ingesting, 2016, and vision system D8 variants. Additionally, several intermediate steps are shown that illuminate the contributions from various technology packages. The morphing steps proceed outward along the line from the origin; the location of each point shows the fuel/noise benefit from the addition of each specific technology. The green and blue line shows key morphing steps leading to the D8 vision system. Several branches off this chain are shown in black, representing variants of interest. The NASA STSLM mid-term goals are shown as the blue shaded areas. The red dot corresponds to the non-ingesting D8, the blue dot is the 2016 D8, and the green dot is the D8 vision system. Table 3 summarizes key parameters of each of these

Parameters	TASOPT 737-800	TASOPT 737-800 OPT.	TASOPT UW-D8-2016	TASOPT D8-2016	TASOPT D8-2035
PFEI (kJ/kg-km)	8.72	7.80	6.16	5.43	3.19
MTOW (lb)	173,790	157,053	133,700	127,935	107,250
Mission Fuel (lb)	47,349	42,491	33,688	29,681	16,059
Baseline Fuel (%)	111%	100%	79.3%	69.9%	37.8%
L/D (-)	16.9	16.8	16.8	17.9	20.1
W/S (lb/sqft)	124	122	116	116	124
TSFC (lb/hr/lb)	0.612	0.601	0.551	0.533	.410
FPR (-)	1.69	1.69	1.49	1.44	1.47
BPR (-)	5.1	5.1	8.5	9.1	20.0
Altitude (ft)	34786	36007	38204	37235	37080

Table 3. Key parameters resulting from D8 morphing study

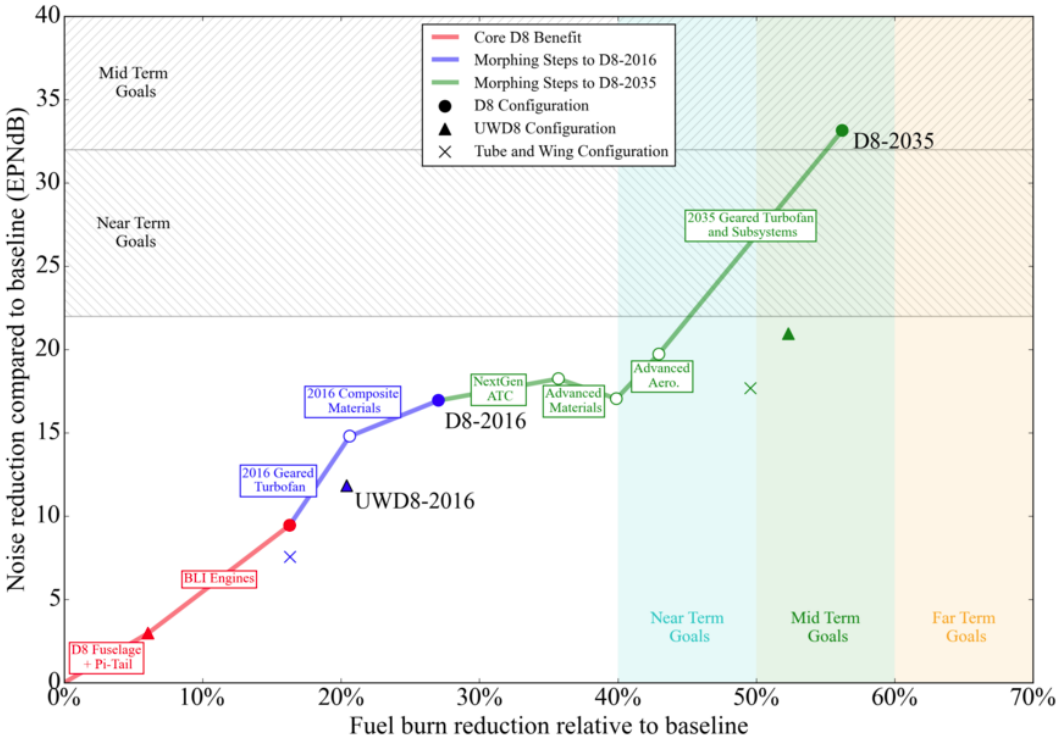

Fig. 6. Morphing steps leading to the different D8 variants

vehicles, as well as the baseline aircraft. Relative fuel burn is also included.

A key piece of information in Figure 6 is the core benefit of the D8 configuration, shown as the green line. This fuel burn benefit, 20.6%, is unique to the D8. Of that 20.6%, 7.7% is due to the D8 fuselage and pi-tail, and 12.9% is due to the integration of the engines with the airframe.

While the widened fuselage improves lift-carryover efficiency and provides a positive pitching moment contribution which reduces the required horizontal tail size, the L/D of the non-ingesting D8 is similar to that of the baseline configuration because the reduced horizontal tail size is approximately offset by increased wetted area of the fuselage (due to the non-cylindrical shape). The non-ingesting D8 offers a 21% fuel burn benefit over the baseline aircraft – which again is the TASOPT-optimized Boeing 737-800.

Table 4 shows that there is some dependency on the ordering of the technology benefits. Composite materials have more of an effect on the 2016 D8 due to the longer fuselage required to accommodate the BLI engines, while the fuel benefit due to the introduction of geared turbofan technology is smaller with BLI. The opposite is true for the noise benefit.

Balanced field length for the D8 is constrained to be less than or the same as the Boeing 737-800. However, the potential for shortening that distance does exist and was

Parameters	TASOPT UW-D8-2016	TASOPT D8-2016
D8 Fuselage and Pi-Tail	7.7%	7.7%
Current Generation Composites	5.6%	6.0%
2016 Geared Turbofan Engines	7.4%	3.5%
Boundary Layer Ingestion	-	12.9%
Total Benefit	20.7%	30.1%

Table 4. The source of the fuel burn benefit for the 2016 and non-ingesting D8 variants

considered as part of N+3 Phase I. Figure 7 shows a variant of the D8 that is constrained to a 5000ft balanced field length. This aircraft has a significant penalty in fuel burn but does yield a potential noise reduction benefit. The noise benefit is due to the lighter wing loading required to meet the takeoff performance (98 lb/ft^2 relative to 116 lb/ft^2). This has the effect of lowering approach/stall speed for a given approach angle and thus reducing aerodynamic noise. Higher fidelity source-noise characterization is a candidate for future work.

The other key D8 variant, the D8 Vision System, offers a substantial improvement over the 2016 D8. This is not due to any additional unique features of the airplane but rather due to the integration of future technology forecasting into the 2035 timeframe. The technology improvements that go into the D8 Vision System are grouped into four categories: operational improvements, advanced aerodynamics, advanced materials, and advanced propulsion and power subsystems. The Boeing SUGAR Phase I report [18] is the source of these technology forecasts. The integration of all of these benefits, which are discussed in detail below, yields a 62% fuel burn reduction compared to the baseline, as well as a 36 EPNdB noise reduction. This meets or exceeds NASA STSLM goals in these categories.

5 The Aurora D8-2016

5.1 D8 Conceptual Air Vehicle Configuration

The outputs from the sizing and optimization results of TASOPT for the 2016 variant of the D8, D8-2016, formed the basis for the design activities. In this section, the details of the Aurora D8 design and its key characteristics are presented and discussed. Emphasis is placed on design challenges unique to the D8 and potential solutions to these challenges.

The conceptual design solution resulting from this D8 design study is presented in Figure 7, where the general arrangement, passenger cabin layout and fuselage cross-section are shown. The defining features of the D8 configuration are clearly identifiable in (i) the unique double-bubble fuselage which creates more lift than a traditional cylindrical fuselage, improves lift-carryover performance, and results in an operationally favorable twin-aisle configuration; and (ii) the aft-mounted boundary-layer ingesting propulsion system, which improves both airframe and propulsion system performance.

The majority of the airframe structure consists of carbon-fiber reinforced polymer (CFRP), and a structural layout was created assuming 2016 composite materials and technologies. The structural components were sized based on the critical load cases and this sizing process was used to produce a bottoms-up estimate of the airframe structural weight. The aircrafts maximum operating speed and Mach number are 340 KEAS and 0.85 respectively, with a typical cruise Mach number in the range of 0.74-0.80.

The D8 fuselage layout was modified from the TASOPT output to allow for 180 passengers in a single-class arrangement with an industry standard 32-inch seat pitch in a 2-4-2 arrangement, while complying with emergency egress requirements. Overhead bins, galleys, and lavatories that meet current standards were also integrated into the floor plan. Although the aft fuselage extends further behind the passenger cabin than for aircraft with underwing engines, the eight-abreast seating results in a shorter cabin than single-aisle aircraft and the aircraft length overall is comparable to current generation, single-aisle aircraft.

The cockpit for the Aurora D8-2016 is largely conventional and accommodates two pilots in a traditional configuration. The flight control system is digital fly-by-wire with envelope protection. Due to the distinctive upturned nose which creates more lift and pushes the fuselage center-of-pressure forward fuselage to reduce the required tail download, an artificial or synthetically augmented vision system may be necessary. However, the cost of synthetic vision system is thought to be outweighed by the benefits of the upturned nose which is of the

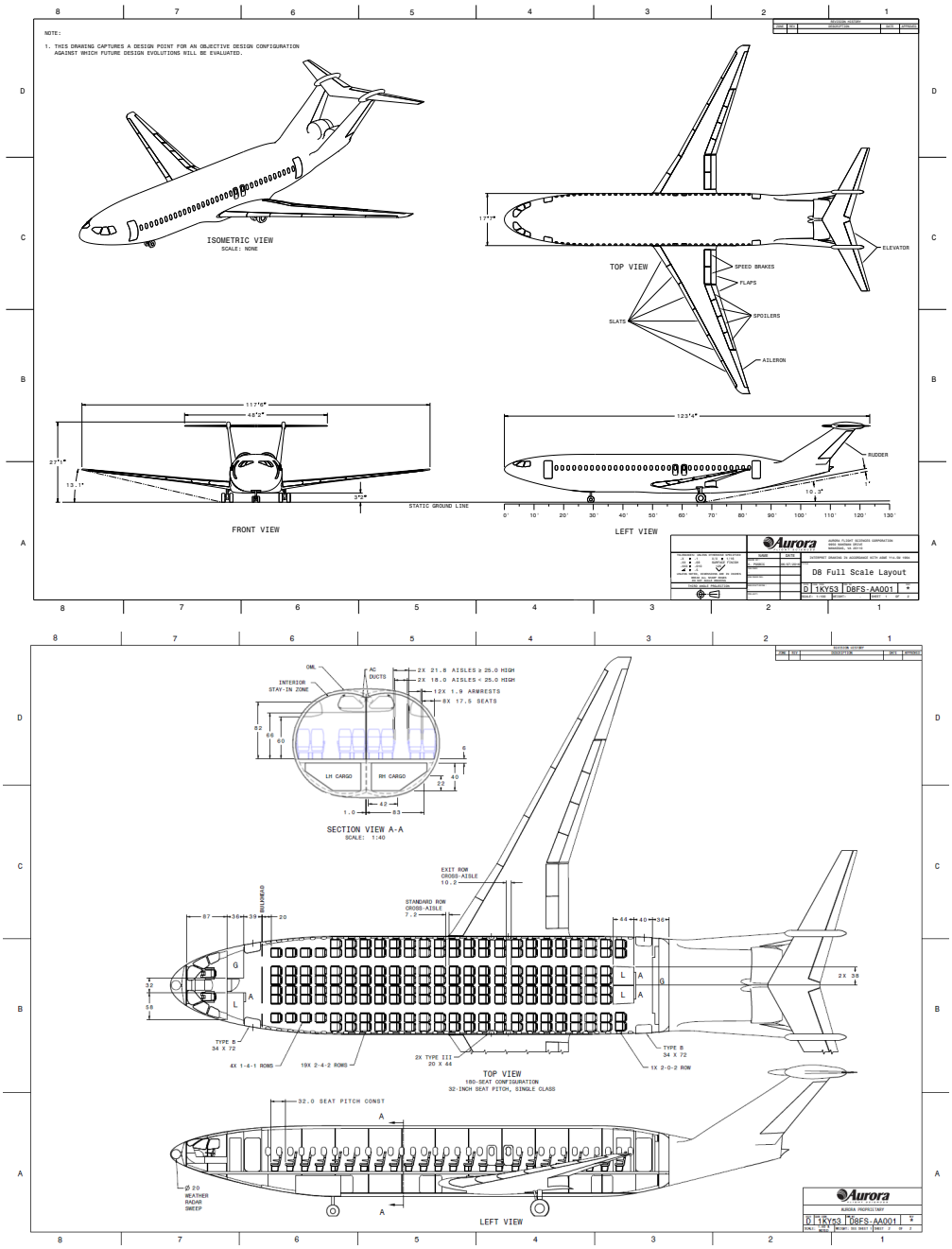

Fig. 7. D8 general arrangement (top). Internal profile in a single-class configuration (Bottom).

order of ΔC_{m0} = 0.05 compared to a more conventional cab design.

Visually, the D8-2016 is more similar to traditional single-aisle concepts than the MIT N+3 Phase I D8 due to the higher cruise Mach number for the Aurora D8 variant, which results in a more conventional, span-constrained wing. The basic planform is trapezoidal, with an extended wing root chord to provide ample fuel volume and to accommodate the main landing gear. Modern supercritical airfoils are used to define the wing loft with thickness and camber variations along the span to obtain the desired swept isobars on the upper surface and a satisfactory span load distribution. The high-lift system of the D8-2016 is also relatively conventional with a system similar to current generation aircraft, consisting of full-span slats at the leading edge and partial span double slotted Fowler flaps at the trailing edge. When sizing the aircraft, the maximum lift coefficient in takeoff configuration was assumed to be 2.0 and in landing configuration it is 2.7. The approach speed is 135KEAS at maximum landing weight.

The lateral control system consists of outboard ailerons and inboard spoilers. Ground spoilers located on the inboard wing provide a means to dump lift quickly upon landing. The main difference between the Aurora D8 wing and current single-aisle tube-and-wing designs is in terms of overall size; The D8 wing is 8% smaller than that of the 737-800.

Weight and balance poses a challenge for the D8 due to the rear engine configuration which results in an aft aircraft empty center of mass relative to the passenger cabin. This leads to a relatively large center of gravity (c.g.) range than aircraft with wing mounted engines. For the D8 configuration this issue is compounded as the engines are mounted at the end of the fuselage rather than near the end of the passenger cabin like traditional rear-engine-mounted aircraft.

It is desirable to have the wing located forward on the body so that the fuel load is centered near the payload c.g., and the loaded aircraft c.g. is generally aft on the mean aerodynamic chord (m.a.c.). However, the wing position is constrained by the need to have the main landing gear behind the empty c.g. in the space behind the wing rear spar. Operators desire an unrestricted passenger and freight loading envelope for operational flexibility, and as a result, much attention was paid to getting a good balance between the conflicting requirements of passenger and freight loading envelope and c.g. position and hence tail size.

To obtain an adequate loading envelope, a relatively forward c.g. in typical operating conditions had to be accepted, and the final loading diagram for the chosen wing position with 180 passengers in single-class seating is shown in Figure 8. A c.g. travel about 50% m.a.c. was established, with minor restrictions on passenger loading. Unrestricted loading requires a c.g. travel of about 52%. The landing gear is relatively aft on the wing at almost 60% m.a.c. As can be seen in Figure 8, during typical operating conditions the c.g. is generally forward—with a full passenger payload, the c.g. varies between about 17% – 22% m.a.c. depending on the fuel load. Normally such a forward c.g. would lead to a large trim drag; however, the favorable forward fuselage lift mitigates this considerably, and the tail download in cruise is quite small.

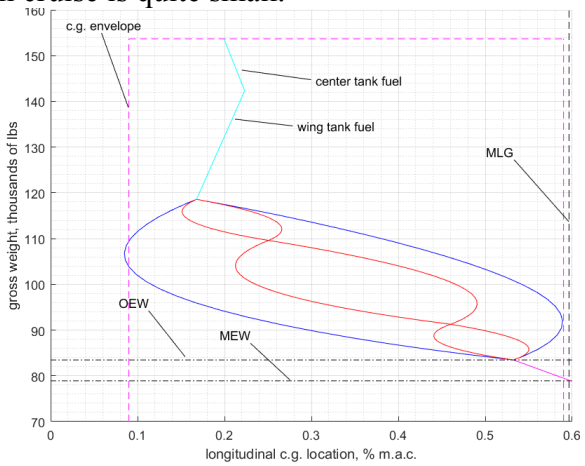

Fig. 8. Aurora D8-2016 loading diagram. The blue curves show c.g. travel for row-by-row loading, and the red curve show loading limits for window-aisle-center seat sequence loading.

Unlike the wing, the empennage is highly unconventional. It is a pi-tail with a swept horizontal stabilizer and twin fins. The horizontal stabilizer incidence is used for trim, and four segments of elevators are the primary pitch control effectors. Each fin has a single segment rudder for directional control. The horizontal tail sizing criteria required that the minimum static margin was no less than 5% m.a.c. and a reasonable tail lift coefficient (-0.7) at forward c.g. on approach. The sizing chart is shown in Figure 9. The minimum tail volume coefficient to satisfy these criteria and to meet the 50% c.g. travel shown in Figure 9 is $V_H = 0.75$. This was used to set the initial tail size for early layouts. As the design progressed towards a reasonable compromise for loadability, the wing was moved forward on the fuselage, but the empennage was not resized as part of the final design spiral. Thus, the aircraft has a much larger tail volume, $V_H = 0.98$, than required, which would allow about 60% m.a.c. travel. The horizontal stabilizer area can be reduced by about 13% and satisfy the minimum tail size requirement. This would result in a weight reduction of about 100lb and a profile drag

reduction of about two counts. This is an obvious area of opportunity for future design cycles.

The propulsion system for the Aurora D8-2016 is a boundary-layer ingestion capable turbofan with core technology and hence thermal efficiency comparable to current best-in-class engines for the single aisle market as of 2016. The propulsion system is aft-mounted on the upper-side of the fuselage and it is assumed that 40% of the fuselage boundary layer is ingested by the propulsion system during cruise flight. The propulsion system cycle was calculated using an Aurora variant of the TASOPT engine model, which is compatible with BLI systems as it is able to account for the propulsive efficiency benefit of the BLI. Simultaneously, the engine-

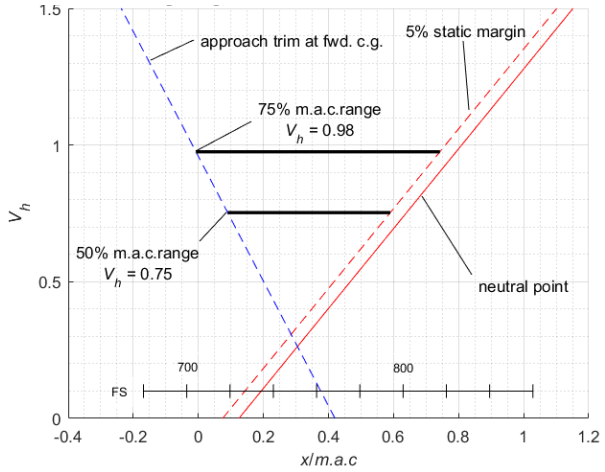

Fig. 9. Aurora D8-2016 tail sizing. The approach trim at forward c.g. and 5% static margin boundaries are shown in blue and red, respectively. Tail volume for 50% m.a.c. range is 0.75.

cycle was designed so that no credit was taken for future enhancements in core technologies or engine weight. A design study was undertaken to determine the optimal fan pressure ratio and engine size for the 2016 D8 and it was found that a twin-engine configuration with two 73 in. fans at a FPR=1.45 provided a suitable compromise between propulsive efficiency, size and weight. Each engine has a sea level static thrust of 24,200 lb. Full details of the propulsion system design study are presented in Section 5.3. The upper aft fuselage, fins and nacelles are integral parts of the fan inlets. A summary of the aircraft's salient characteristics and performance for the design mission is presented in Table 5.

Throughout the design process attention was paid to retaining many of the operational capabilities of traditional tube-and-wing configurations. In addition to the wing-span constraint to retain compatibility with Group III gates, the design was required to retain compatibility with aircraft tugs, ground-handling equipment and jet ways. A CAD model of the Aurora D8-2016 at a gate beside a Boeing 737-800 at a similar gate is shown in Figure 10.

5.2 Airframe Design and Analysis

The D8 airframe design used a NASA/MIT Outer Mold Line (OML) loft [14] as the initiation point for this effort. The point-of-departure OML had been developed for wind-tunnel testing in order to investigate aerodynamic and propulsion benefits of the configuration. This model lacked internal structural details.

The conceptual design process required constant iterations across a multi-discipline team. The airframe-centric view of these interactions is

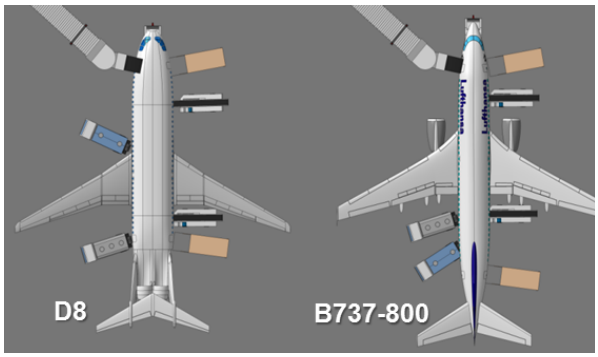

Fig. 10. D8 integrates into existing gate servicing.

illustrated in Figure 11. The computer-aided design (CAD) OML serves as the backbone across the disciplines, with information flowing through the CAD to and from the other disciplines. The CAD geometry is considered the master model. Geometry is exported from CAD in order to generate computational fluid dynamics (CFD) and finite element analysis (FEA) models.

Accommodation	
Flight Crew	1-2
Cabin Crew	3-5
Passengers	180 (single class, 32" pitch)
Capability	
Still Air Range	3000 nm (full pax load)
Long Range Cruise Speed	0.78 Mach
Maximum Operating Mach	0.82 Mach
Maximum Operating Altitude	FL410
Takeoff Field Length	7,750 ft
Dimensions	
Wing Span	117 ft 6 in
Length	124 ft 5 in
Height	25 ft 0 in
Fuselage Width	17 ft 7 in
Wing Area	1,244 sq ft
Cabin Width	16 ft 7 in
Cabin Length	76 ft 4 in
Aisle Height	7 ft 10 in
Aisle Width	18 in
Seat Width	17.5 in
Underfloor Cargo Volume	1,700 cu ft
Propulsion	
High Bypass Turbofan	2 x 73 in. fans
Thrust	24,200 lb (sea level static)
Weights	
Maximum Takeoff Weight	153,670 lb
Maximum Landing Weight	138,303 lb
Maximum Zero Fuel Weight	128,476 lb
Maximum Fuel Weight	41,660 lb
Operating Empty Weight	83,476 lb
Design Mission Performance	
Still Air Range	3000 nm (full pax load)
Initial Cruise Altitude	37,500 ft
Approach Speed	135 KEAS
Takeoff Gross Weight	153,670 lb
Payload	35,095 lb
Block Fuel	29,245 lb
Reserve Fuel	5,850 lb
Landing Weight	124,425 lb
Takeoff Wing Loading	124 psf
Takeoff *T/W*	0.27
Long-range cruise Mach #	0.78

Table 5. Aurora D8-2016 General Characteristics

5.2.1 Airframe Design

Aerodynamics drive the D8 configuration to have an up-swept nose, as described in detail in Section 5.3.1. One of the considerations discovered during this work is the impact of this geometry on the pilot visibility out the cockpit windscreens. FAR 25.775 and AC25.773-1 [19] provide guidance regarding required pilot visibility. For this study, a 95th percentile male pilot is placed at a nominal location within the cockpit. View angles in compliance of

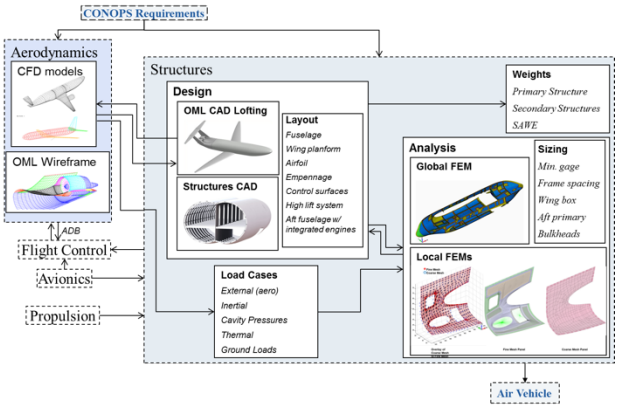

Fig. 11. Airframe design and analysis method

AC25.773-1 are modeled and cockpit windscreen geometries are defined. Three nose variants are considered, as illustrated Figure 12. The -101 variant is the nominal aerodynamic nose, -103 enables the windscreens to be fully-compliant with view requirements, and -102 is a compromise between the -101 and -103 variants. The forward pressure bulkhead partially interferes with the field of view looking straightforward. An illustration showing the interference from within the cockpit for the three nose variants is shown in Figure 12. The conceptual design presented in this paper maintains the OML with the maximum aerodynamic benefits (i.e. -101) described in Section 5.3.1, as it is anticipated that methods for supplementing the pilot with optical cameras will be accepted in the near future. For example, Gulfstream recently earned certification for an Enhanced Vision System [20]. A conceptual layout of the D8 cockpit is completed was part of this study; ample space is available for placement of modern, large multi-functional displays.

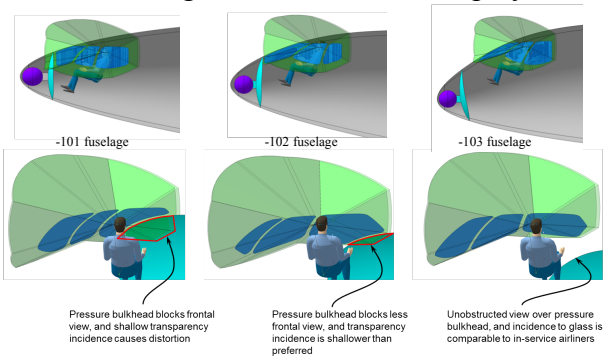

Fig. 12. FAR25.775 and AC25.773-1 visibility study

The size of the fuselage was grown slightly from the NASA/MIT point-of departure OML in order to accommodate 180 passengers while complying with emergency egress requirements and offering an industry standard 32-inch seat pitch. The latest in passenger seats is used as the base for the seat dimensions. Seat cushions are 17.5 inches wide and armrests are 1.9 inches wide for an effective seat width of 19.4 inches. The aisles are 18 inches wide from the floor up to 25 inches above the floor. Above 25 inches from the floor, the aisles are 21.8 inches wide. FAR 25.775 requires 15 inches and 20 inches, respectively. To accommodate the aisles widths and seat widths, the fuselage width grew slightly from the point-of-departure model. A view of some of the conceptual passenger considerations is shown in Figure 13. Overhead baggage space allows for one carry-on bag for every passenger.

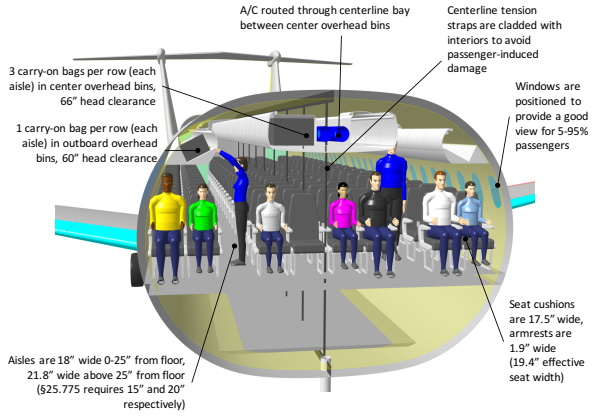

Fig. 13. Partial list of D8 passenger human-factors considerations

Unique to the D8 configuration is the centerline structural elements that run down the middle of the fuselage and connect the upper fuselage skin to the lower fuselage skin. The conceptual function of a central element is to provide a load path from upper skin to lower skin in order to reduce bending stress, and therefore, structural mass and deflection of the fuselage skins along the upper and lower cusps, Figure 14. As incorporation of structure down the middle of a fuselage is an unconventional approach, a trade was performed to investigate the central element design space from simple tension rods located at each frame station to a full-height shear web (i.e. wall) with cutouts separating the left and right lobes of the fuselage. A third consideration was a hybrid of the two previous concepts, merging tension rods with partial-height shear webs.

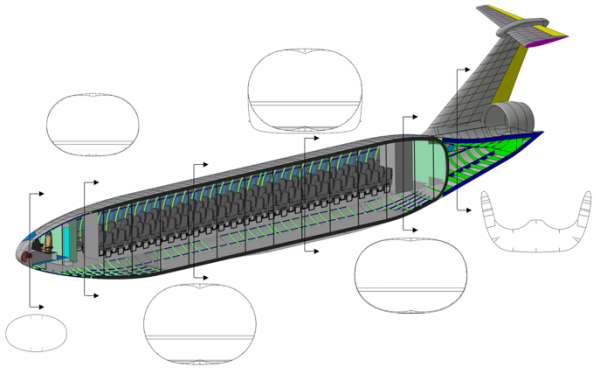

Fig. 14. D8 fuselage section cuts

The three central element concepts, tension rods, tension rods with a partial web, and a full-height web with cutouts, were evaluated for suitability on the D8, and those results were reported out in Reference [21]. The trade study found two main results: (i) the dual-lobed cross-section is more mass efficient than an oval or elliptical fuselage, and (ii) including structure to tie the cusp of the fuselage along buttline zero decreases the total structural mass. While the full-height web and tension rods with partial web design weights were relatively similar from a mass-efficiency standpoint, periodic tension rods offer greater cabin configuration flexibility. In addition, bending is a driving sizing factor for the fuselage. There is diminishing returns to having a full height central web with mass near the neutral axis of the fuselage. The chosen solution is a tension rod with a longitudinal keel beam (shear web), as demonstrated in Figure 15 and described in detail in [21].

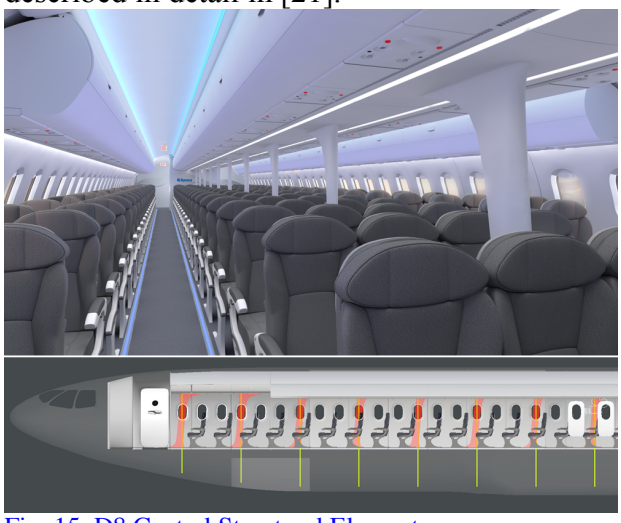

Fig. 15. D8 Central Structural Elements

The standard row cross-aisle spacing (from seat-back to seat cushion) is 7.2 inches. For the emergency exit rows, the cross-aisle spacing is 10.2 inches. Galley, lavatories, and service doors (Type B) are included in order to set the fuselage length. In order to comply with FAR requirements, the fuselage length slightly increased from the point-of-departure OML. The D8 airframe is comprised of five major components; fuselage, aft fuselage, wing, vertical stabilizers, and horizontal stabilizers. The airframe utilizes a traditional composite fuselage build approach, utilizing frames and stringers in the fuselage and aft fuselage, and spars, ribs, and stringers in the wing, vertical stabilizers, and horizontal stabilizers. However, the fuselage adds a unique central element, the Y-clip, keel, and tension rods as described above. As with traditional passenger aircraft, the D8 has a mix of pressurized and unpressurized bays. Figure 16 (top) illustrates the conceptual design of these bays.

The structural arrangement for the fuselage utilizes a typical frame spacing between 20 and 24 inches. Windows are placed within the frame bays throughout the passenger cabin. The frame pitch is decreased in the surrounds of doors and emergency exits as well as in the region of the wing carry-through structure. The fuselage skin has integrated hat stiffeners running along the length of the aircraft. The main fuselage cabin has a forward and an aft pressure bulkhead. The nose landing gear and the wing carry-through structure bays are reinforced pressure bulkheads. The fuselage also contains cargo doors. The floor structure of the fuselage provides support for the passenger cabin. Continuous seat tracks and seat track beam caps run across the top of the crossbeams. Hat shaped seat track beams are discontinuous at every crossbeam. Shear clips tie the vertical support struts to the seat track beams and cross beams. Six inches of depth is allotted for the floor structure (0.5 inch for seat track and floor boards, 5.25 inches for seat track beams and cross beams, 0.25-inch margin for miscellaneous). The depth of the floor allows for the calculation of the D8 cargo volume. A volume comparison between the D8 and a Boeing 737-800 is shown in Figure 16 (bottom); the D8 has slightly more cargo volume than the Boeing 737-800. Note, only half of the rear cargo hold volume is included for the D8. It is

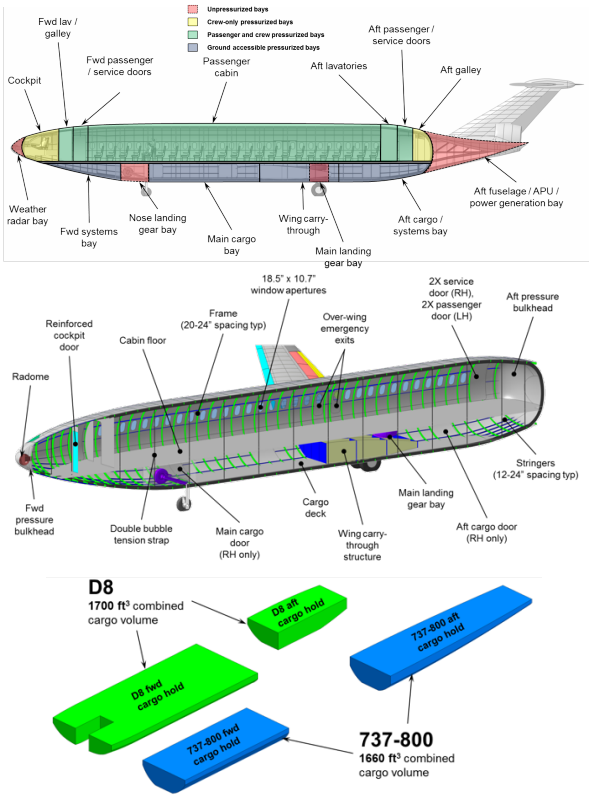

Fig. 16. D8 fuselage structural arrangement. Pressurized and unpressurized sections (top), interior structural concept (middle), and available cargo volume (bottom).

envisioned some aircraft systems will potentially occupy the other half of the rear cargo hold volume. This assumption should be reassessed as the D8 concept moves beyond the conceptual design state. In addition, a cargo floor structure may be required in order to avoid the Y-clip and central keel in the lower hold.

The D8 wing, as shown in Figure 17, is free of engines and conventional in relatively every way; the structural layout follows typical practice. The structure consists of three main spars running the length of each wing. These spars tie into the wing carry-through structure (that passes through the underside of the fuselage). Each wing has ribs at a typical spacing between 20 and 24 inches. The models include simple geometry for the high-lift devices. The main landing gear pivot point is just outside the fuselage with the gear pivoting inward to stow below the fuselage. An additional spar boxes out the main landing gear bay. The wing contains 6 degrees of dihedral to provide landing clearance in the cross-wind landing case.

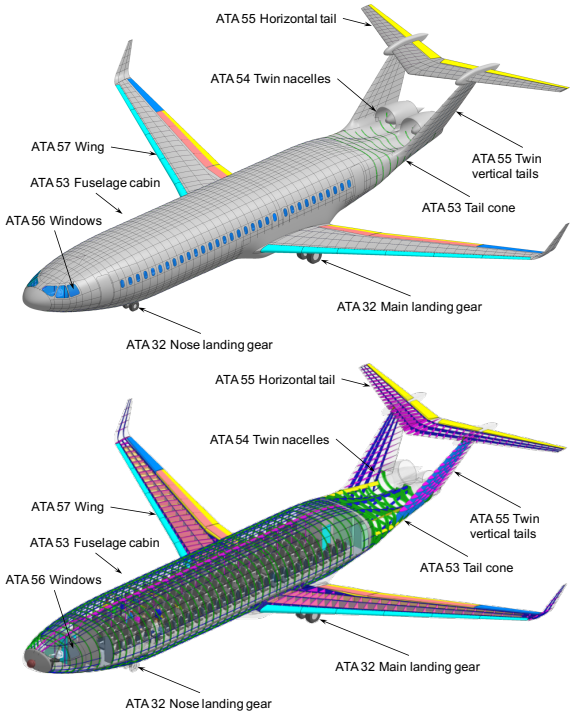

Fig. 17. D8 structural layout

The D8 aft fuselage requires unique structural design solutions in order to integrate the engines as well as for the pi-tail. The aft fuselage and stabilizers follow the same design methods as the fuselage and wing. The structural layout for the aft fuselage and empennage is shown in Figure 18. The aft fuselage is comprised of hoop frames with hat-stiffened skins. In addition to the hat stiffeners, longerons/keels provide additional capability to react the forces from the empennage and engines. For the vertical and horizontal stabilizers, three main spars run their length with typical rib spacing between 14 and 16 inches.

In this conceptual design, the point-of-departure propulsion system architecture is designed by Pratt & Whitney (P&W) with the goal of being compliant with the UHERF 1:20 regulation [22]. Two powerplants are located side-by-side and employ an innovative reverse-flow gas generator core. Each core exhaust drives a low-pressure turbine which is mechanically linked to each fan via a gearbox. The flow in the low-pressure turbine is turned back to streamwise inside the fan exit guide vanes and exhausted at the trailing edge. A choice is yet to be made as to whether the fans are of co- or counter-rotating design relative to one another. To prevent fratricide and reduce exposure to the

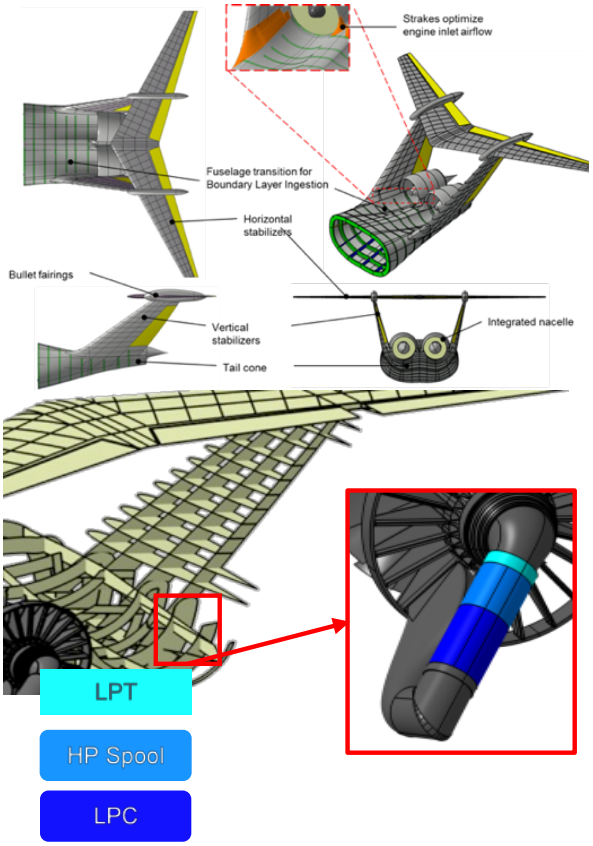

Fig. 18. D8 conceptual empennage design. General arrangement (left), and reverse-flow engine installation (right).

empennage structure and critical systems in the event of an uncontained rotor burst, this possible solution mounts the engine cores at approximately 45 degrees to aircraft axis with the flow path reversed to that of the fans. An illustration of the potential P&W reversed-flow core design installed on the aircraft is shown in Figure 18 (right). A conceptual-level UHERF study was performed in order to assess the potential of the reverse-flow architecture; sacrificial spars are currently accounted for in the vertical tails. More details of this potential D8 powerplant installation can be found in Reference [13].

5.2.2 Airframe Analysis and Weight Estimation

The D8 airframe analysis uses the CAD models discussed in Section 5.2.1 as the initiation point. The analysis models of the D8 are the first structural analysis models created for the D8 (i.e. no previous detailed analysis models exist). Model fidelity continues to increase and evolve as the design progresses. The analysis development process begins with the development of the D8 Global Finite Element Model (GFEM). The D8 vehicle is divided into four break-out models, as shown in Figure 19, with the fuselage serving as the integration point of the GFEM. Detailed views of the aft fuselage and vertical tails model and of the fuselage model are shown in Figure 19, where the color map indicates the resolution of property optimization for the global models (i.e. each color can have a unique composite laminate). Sizing of the primary structural elements are based on critical sizing load cases.

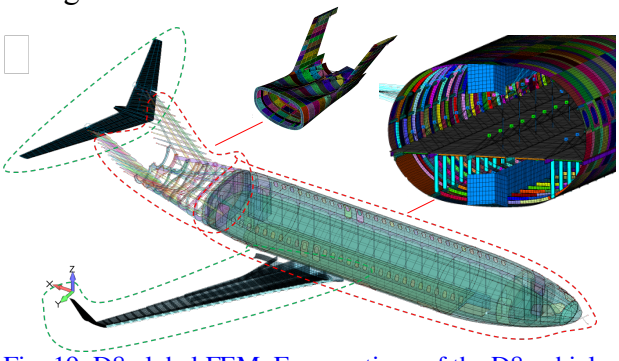

Fig. 19. D8 global FEM. Four sections of the D8 vehicle were used for finite element analysis (bottom left). Detail views of the more complex structures (top right).

Load case generation to support the conceptual design of the D8 requires identification of critical sizing load cases which are a subset of the many thousands of load cases typically analyzed during a detailed design phase. Literature, such as NASA G-7123.1-001 [23] was reviewed in order to identify typical critical load cases to consider during the conceptual design phase. In addition, FAR Part 25 was consulted along with in-house Aurora expertise. From these sources, a preliminary master list of load cases is compiled in Table 6.

The GFEM and trade study models follow the same methodology whereby CAD generates geometry that is meshed and solved in NASTRAN before structural optimization is carried out within Hypersizer. FEM generation begins with geometry generated from the CAD. The geometry is meshed and material properties and sections are assigned within FEMAP. Load cases are assigned and the model is analyzed in NASTRAN. The FEM and element level results are passed into Hypersizer, where the sections are optimized to generate the minimum-weight solution that satisfies minimum-margins of safety. Hypersizer generates a new file containing the optimized properties for the FEM sections. The user can reanalyze the FEM with the new properties in order to check for load redistribution in the optimized configuration. The exchange between NASTRAN and Hypersizer can be iterative, depending on the desired level of optimization. A flowchart illustrating the process used for the D8 analysis studies is shown in Figure 20.

Two methods are used to estimate the weight of the conceptual D8 aircraft: the weight module in NASA's Flight Optimization System (FLOPS) code [24] and an Aurora developed bottoms-up weight estimation MATLAB code. The FLOPS method for estimating structures, systems, and propulsion weights includes a full mission performance analysis. Performance outputs from the TASOPT model along with geometric data from CAD layouts are used as inputs in the FLOPS weight module. Additionally, design range is specified in the FLOPS configuration module to allow FLOPS to calculate takeoff gross weight and ensure enough available fuel to complete the desired mission.

Load Case	Description	Ultimate SF
1	+2.93g MTOW	1.5
2	-0.93g MTOW	1.5
3	4.34g OEW	1.5
4	-2.34g OEW	1.5
5	2g taxi bump MTOW	1.5
6	+2.93g MTOW + 12 psi cabin over-pressure decompression	1.5
7	-0.93g MTOW + 12 psi cabin over-pressure decompression	1.5
8	4.34g OEW + 12 psi cabin over-pressure decompression	1.5
9	-2.34g OEW + 12 psi cabin over-pressure decompression	1.5

Table 6. Fuselage Cross-Section Trade Study Critical Sizing Cases

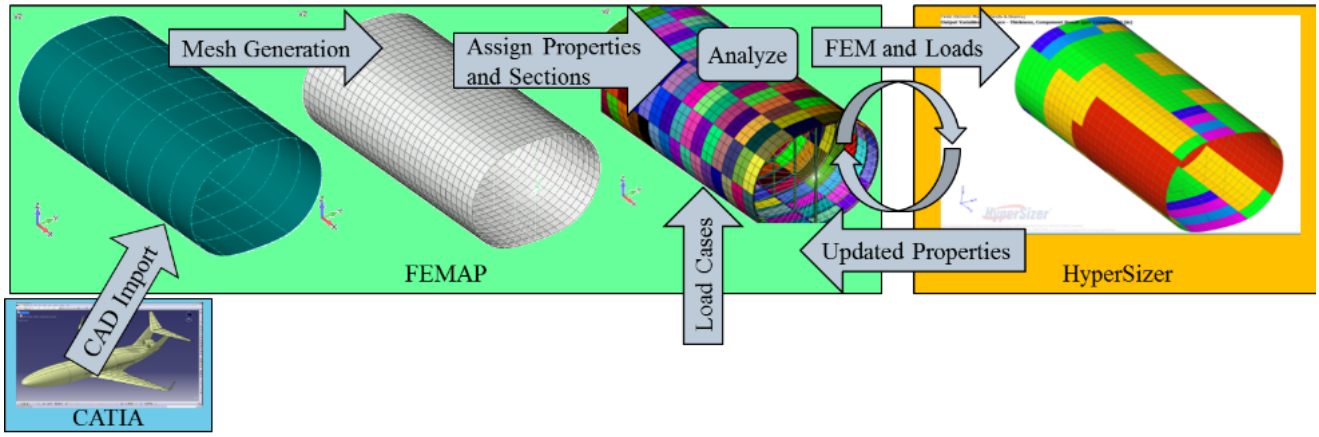

Fig. 20. Typical finite element model generation and analysis flowchart.

Other important assumptions in the model inputs included a mostly composite structure and an advanced technology wing. Furthermore, propulsion parameters are calculated based on an engine deck generated by NASA using TASOPT model outputs. Key results from the FLOPS model are listed in Table 7. The bottoms-up method for estimating structures, systems, and propulsion weights are independent of TASOPT and FLOPS. To estimate airframe structures weights, a bottoms-up approach is employed in which weights are calculated for detailed airframe components. Systems weights are calculated using equations and heuristics from Raymer [25], Roskam [26], and NASA that were developed primarily based on historical data. Propulsion weights are estimated using a combination of textbook equations and information provided by Pratt and Whitney.

MTOW (lb)	145,954
OEW (lb)	81,384
Mission Fuel (lb)	29,469
Block Fuel (lb)	25,842
Wing Area (ft^2)	1,297
Wing Span (ft)	118
Wing Aspect Ratio	10.75
Wing Loading (lbf/ ft^2)	113
Thrust to Weight	0.367

Tab. 7. Key FLOPS Outputs

A code is developed in MATLAB to calculate the D8 airframe structures weights using a bottoms-up approach. Airframe structures are broken down into detailed components, and weight estimates are determined for each part. After completion of the GFEM analysis and optimization, sizing of components updated. This sizing information is used in the MATLAB weight estimation code alongside surface areas and perimeters of sectioned components from CAD layouts. Using this code, detailed component weights are estimated and subsequently classified by ATA codes for consistent bookkeeping. Table 8 lists the rolled-up airframe structures weights.

The systems weights are grouped by their respective ATA chapters, and the resulting high-level weights are shown in Table 9.

Some powerplant weights such as engine controls, exhaust, and nacelle systems weights are estimated using the same method described in the airframe systems weight section. To calculate dry engine weight for the reverse flow engine, known weights of existing engines are compiled, and TASOPT models are run with modifications for future technology levels. Based on the results of these models, the new engine weight is estimated and corrected for current generation technology. The full power plant weight summary is listed in Table 10.

Key aircraft weight estimates for the D8, including manufacturer's empty weight (MEW), operational empty weight (OEW), maximum zero fuel weight (MZFW), and maximum takeoff weight (MTOW) are shown in Table 11. Payload weight includes passenger and crew weight and is allocated based on the FAA AC 120-27E [15] passenger winter weight guideline of 195 pounds per passenger including baggage. Additionally,

ATA Chapter	ATA Title	Current Best Estimate (lb)
50	Cargo and Accessory Compartments	21
52	Doors	2,369
53	Fuselage	12,213
54	Nacelles/Pylons	1,036
55	Stabilizers	2,666
56	Windows	880
57	Wings	14,211
	Total Airframe Structures	33,396

Table 8. Summary of D8 Airframe Structures Weight Estimates

ATA Chapter	ATA Title	Current Best Estimate (lb)
21	Air Conditioning	1,761
24	Electrical Power	3,726
25	Equipment/Furnishings	12,775
27	Flight Controls	1,878
28	Fuel	734
29	Hydraulic Power	609
30	Ice and Rain Protection	328
31	Indicating/Recording Systems	559
32	Landing Gear	5,354
35	Oxygen	166
36	Pneumatic	421
38	Water/Waste	119
42	Integrated Modular Avionics	1,862
49	Airborne Auxiliary Power	1,238
	Total Airframe Systems	31,530

Table 9. Summary of D8 Airframe Systems Weight Estimates

ATA Chapter	ATA Title	Current Best Estimate (lb)
71	Power Plant	1,036
72	Engine Turbine	10,200
76	Engine Controls	226
78	Exhaust	1,255
Total Power Plant (2 Engines)		12,717

Table 10. Summary of D8 Power Plant Weight Estimates

mission fuel weight is calculated from the TASOPT performance model output. To validate the bottom-up weight estimates, results from FLOPS, TASOPT, and a FLOPS weight estimation of the Boeing 737-800 are compared against the design current best estimate. The current best estimate MTOW (153,670 lb), falls within 5 percent of the FLOPS MTOW (145,000 lb), and both are lower than Boeing 737-800 MTOW (174,000 lb), as expected. The TASOPT weight estimate is lower than the design and FLOPS estimates. Taking a closer look at the individual weight categories, the primary discrepancy lies in the airframe structures weight estimates.

Group	Current Best Estimate (lb)
Total Airframe Systems	31,530
Total Structures	33,396
Total Power Plant	12,717
MEW	77,643
Total Operational Items	4,573
OEW	82,216
Total Payload Weight	35,100
Zero Fuel Weight	117,316
Mission Fuel	36,354
MTOW	153,670

Table 11. Summary of D8 Current Best Weight

5.3 Propulsion System Design and Analysis

Propulsion for the boundary-layer ingesting variants of the D8 is provided by two aft-mounted, boundary-layer ingesting, turbofan engines. The engines are mounted in this location to ingest the boundary layer that develops over the D8 fuselage. The BLI capable variants of the D8 include a distortion tolerant fan design which is capable of operation in the presence of the distorted ingested flow.

There are three direct aerodynamic benefits to embedding the air-vehicle's propulsion system in such a manner: (i) Ingestion of the boundary-layer results in an increase in propulsive efficiency, η_{p}, at a given specific thrust, F_{sp}, due to a direct reduction in jet dissipation, Φ_{jet}; (ii) ingestion reduces the aircraft wake which reduces the losses dissipation in the vehicles wake (sometimes referred to as wake-filling); and (iii), an embedded installation naturally leads to a reduction in wetted-area because of smaller nacelle area. These three direct benefits which directly reduce fuel-burn for a given mission are compounded at the system-level to drive down overall vehicle size and weight [7].

While the theoretical benefits of propelling an air-vehicle with BLI have long been known [27], only recently have computational tools and methods become available to design an integrated vehicle on which to maximize the benefits of ingestion. Importantly, the propulsion system must be specifically designed to operate in a highly-distorted flow across the envelope of the vehicle. A design which operates in highly distorted flow across much of its operational envelope is very different from most traditional propulsion system designs where high levels of distortion are only encountered at the corners of the envelope such as cross-wind take-off. As a consequence, an entirely new design philosophy is required for a distortion tolerant propulsion system.

The direct benefit of BLI from the propulsion system perspective is the inherent increase in propulsive efficiency that results from making the propulsor ingest low-energy flow. An increase in propulsive efficiency is achieved because the ingested kinetic energy defect – lower incoming velocity at the inlet – leads to a lower jet velocity for a given mechanical power input, P_K, into the flow:

$$P_K = \frac{1}{2}\dot{m}\left(V_{\mathrm{jet}}^2 - V_\infty^2\right) - \frac{1}{2}\dot{m}\left(V_{\mathrm{inl}}^2 - V_\infty^2\right) \qquad (1)$$

and a lower jet velocity leads directly to reduced jess losses via

$$\Phi_{\mathrm{jet}} = \frac{1}{2}\dot{m}\left(V_{\mathrm{jet}} - V_\infty\right)^2. \qquad (2)$$

The effect of boundary-layer ingestion on propulsive efficiency is plotted in Figure 21, where propulsive efficiency, η_p, is shown on the ordinate and fan pressure ratio, FPR, on the abscissa. Two levels of ingestion are shown: No ingestion, $f_{\mathrm{BLI}} = 0$, i.e., a conventional podded installation is shown in blue and a typical level of ingestion, $f_{\mathrm{BLI_f}} = 0.\ 4$, 40% of fuselage boundary-layer ingested, is shown in red.

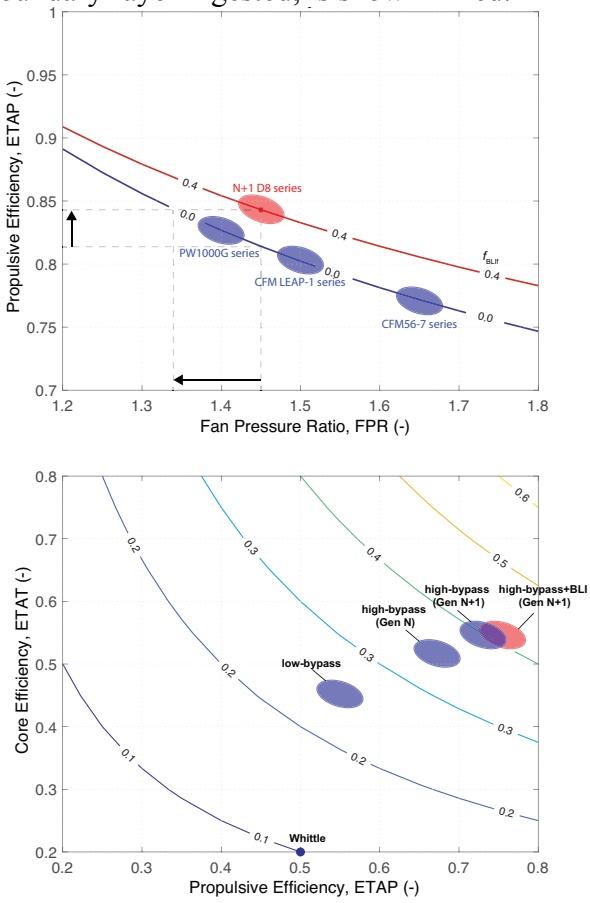

Fig. 21. Effect of OD8 levels of boundary-layer ingestion on propulsive efficiency (top) and overall efficiency (bottom)

The contour presented for no ingestion is the canonical variation of propulsive efficiency with FPR or specific thrust for a podded installation that can be found in any propulsion system textbook—for example see Kerrebrock Figure 1.1 in Reference [28]—where propulsive efficiency is only a simple function of jet velocity and freestream velocity:

$$\eta_{p,f_{\mathrm{BLI}}=0} = \frac{2}{1+\frac{V_{\mathrm{jet}}}{V_\infty}}. \qquad (3)$$

This equation illustrates why there has been a trend for ever lower FPR (lower specific thrust) as the commercial jet-age has progressed: the continuous drive for higher efficiency has driven us further to the left on the blue curve in Figure 21 (top). This historical trend towards lower specific thrusts is shown in Figure 21 (bottom) by the addition of some single-aisle propulsion systems along the blue curve.

For a given thrust requirement, however, a lower specific thrust requires a larger engine to pass the necessary mass flow. These lower specific thrust engines are therefore larger, and, as a result, are heavier and have larger wetted areas than higher specific thrust designs. Hence, a compromise must be made between higher propulsive efficiency, and increased weight and external drag. To minimize the negative impacts of external drag and weight improved integration design and advances in materials for weight savings have been major focuses of recent installation efforts.

An alternative to reducing specific thrust further is to ingest the aircraft boundary layer as can be seen from the curve of 40% ingestion shown in red in Figure 21 (top). CFD studies on the D8 configuration have demonstrated that the vehicle ingests about 40% of the boundary-layer during cruise, and, as a result, this curve represents the propulsive efficiency variation possible with the D8. It can be seen that there is a 2–4% direct propulsive efficiency benefit in the presence of 40% ingestion across the range of viable specific thrusts—with a larger benefit achieved at higher specific thrusts.

A trade-space study spanning a portion of the red line was undertaken to determine the optimal FPR for the OD8 for minimum mission fuel over a predetermined 3000 nm mission. Based on the functional variation shown in Figure 21 and estimates of the variation of fan-stage efficiency and fan weight with fan pressure ratio, it was found that an aerodynamic design point fan pressure ratio, FPR = 1.45, provided the best compromise between efficiency, weight, and aft-end integration. This region of optimal FPR for the D8 is included in Figure 21 (top) and it is immediately clear that such an installation would provide a propulsive efficiency above current (2017) best-in-service engines.

To directly compare the D8 BLI installation and traditional podded propulsion system performance, it is useful to define an effective fan pressure ratio which is defined as the FPR that would be required in a non-BLI case to achieve the same propulsive efficiency, i.e.,

$$\eta_p(f_{BLI}=0, FPR_e) \equiv \eta_p(f_{BLI}=f_{BLI}, FPR). \qquad (4)$$

The effective fan pressure ratio is easy to visualize from Figure 21 by taking a horizontal line from the D8 configuration across to the non-BLI line. Using either method it is found that FPR=1.45 for the 2016 D8 is equivalent in terms of propulsive efficiency to a non-BLI fan design at FPR=1.34, but without the associated nacelle weight and nacelle drag penalty that accompany a traditional design in the FPR=1.35 range.

To make sure that no credit for improved engine technologies, aside from BLI performance, are given to the D8 configuration, the engine core efficiency was deliberately maintained at a similar level to current best-in-service engines such as the CFM LEAP 1 series and the PW1000G geared turbofan series. Retaining a similar level of core engine technology allows the benefits of the D8 configuration to be separated from future engine technology enhancements. The propulsion system technology-level for the OD8 was based on current generation turbofan performance and is loosely based on the current generation of geared turbofans produced by P&W. The engine-cycle used for the D8 presented in this paper was computed using Aurora's in-house propulsion system tool which is based off the engine model found in TASOPT. This model was employed

over the more industry standard NPSS because of the ease with which BLI could be integrated into the cycle.

The overall performance of the 2016 D8 propulsion system is demonstrated relative to other engines in Figure 21 (bottom), where propulsive efficiency is plotted versus core efficiency for various engines. This figure is adapted from Reference [6]. The figure simultaneously illustrates both the propulsive efficiency benefit associated with BLI and the comparable engine core efficiency to current best-in-class engines. With a propulsive efficiency of 0.75 and a core thermal efficiency of 0.55, the overall efficiency of the propulsion system is 0.413. Based on these engine parameters, the propulsion system was sized based on the thrust requirements at take-off, top-of-climb and cruise. The key parameters of the power-plant are presented in Table 12.

For the purpose of this design study no attempt was made to design a distortion tolerant fan. This area is the subject of a significant amount of ongoing research, particularly the design of a D8 X-Plane flight demonstrator, which will be reported out in subsequent literature. Instead, for this study it has been assumed that a distortion tolerant fan could be developed to work in the environment created by the D8 configuration. To account for the design compromises that would be required to produce a propulsion system that could operate effectively in the BLI environment of the D8, a 1.0% fan-stage efficiency debit was included relative to current generation fan performance.

One installation variant for the D8 configuration propulsion system involves an innovative reverse-flow gas generator core. Each core exhaust drives a low-pressure turbine which is mechanically linked to each fan via a gearbox. The flow in the low-pressure turbine is turned back to streamwise inside the fan exit guide vanes and exhausted at the trailing edge. To prevent fratricide and reduce exposure to the empennage structure and critical systems in the event of an uncontained rotor burst, one possible solution is to mount the engine cores at approximately 45 degrees to aircraft axis with the flow path reversed to that of the fans. An illustration of the proposed P&W reversed-flow core design is shown in Figure 18.

5.4 Aerodynamic Design and Analysis

The D8 boasts distinct aerodynamic configuration differences from the traditional wing-tube aircraft which contribute to the D8's overall efficiency. The main features are the wide-body, “double-bubble" fuselage, the Pi-tail, and the aft, flush-mounted, BLI propulsors. Early conceptual aerodynamic work was conducted to assess these features. Other aero-efforts also included developing a traditional drag-build up to estimate aerodynamic performance of the D8 in the absence of a detail-designed geometry.

CFD studies, which were conducted in Star-CCM+, focused on (i) investigating the fuselage contribution to the lift and moment benefit, and (ii) evaluating initial designs of the aft-end integration. In addition to the CFD effort to assess configuration changes to the D8, a low-

Parameter	Value
General characteristics	2 x 73 in. fans
Thrust (Seal Level Static)	2 × 24,200 lb (2 x 102 kN)
Equivalent shaft power (sea level static)	2 x 20,800 shp (2 x 13.0 MW)
Operating pressure ratio (OPR)	40
Bypass ratio (BPR)	10
Fan pressure ratio (FPR)	1.45
Cruise TSFC	0.535 lb/hr/lb
Overall cycle efficiency	0.413
Weight (dry, each)	5,100 lb (2,310 kg)

Table 12. Key engine parameters

speed, unpowered wind tunnel test was conducted in August 2016 on a 5%-scale D8 at the 12-ft Low Speed Tunnel in NASA Langley [29]. The main goal of this wind tunnel test was to investigate the low-speed longitudinal and lateral characteristics of the D8 and understand how the aerodynamics change due to design changes to nose shape and tail layout. Figure 22 shows the 5%-scale wind tunnel model and all the different configurations including the different control surfaces at various deflection angles, an alternate nose, and various tail layouts.

Fig. 22. 5%-scale D8 wind tunnel model. This model was used in the Aug 2016 D8 configuration wind tunnel test conducted at the 12-ft LST at NASA LaRC. Shown is the nominal OML (fully assembled), alternate tails (low-mounted horizontal tail, tail-off), alternate nose, and control surface [29]

5.4.1 Fuselage Aerodynamics

The shape of the D8 fuselage was designed to provide a greater carryover lift across the span as well as a more positive pitching moment which contributes to the reduction in wing and tail size. A CFD study was conducted on a simplified geometry to quantify these aerodynamic contributions.

To assess the carryover lift, a D8 fuselage-wing geometry was modeled in CFD. As seen in the top graphic in Figure 23, the forward fuselage features the signature D8 wide-body and up-swept nose. Since the goal of this computational study is focused on the fuselage, the vertical tail, horizontal tail, and nacelles were removed for simplicity. In their place, a beaver-tail (lofted tail) was added to ensure clean aerodynamics leaving the body. The wing was kept in the simulations because it is needed to capture the carryover lift.

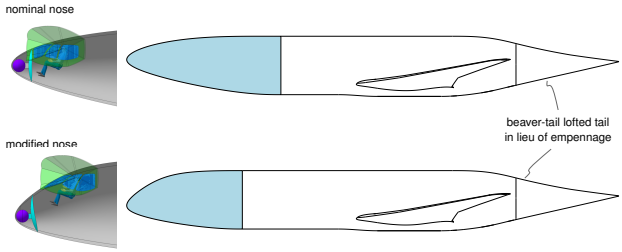

Fig. 23. Geometries used in the CFD assessment of the D8 fuselage effects. Top: Nominal D8 nose that is up-swept. Bottom: Modified D8 nose that features a conventional nose shape similar to the current fleet. Blue-shaded regions highlight the geometric differences between the two configurations. Right side images depict the corresponding equipment packaging and pilot view for each nose shape.

A second fuselage-wing geometry, seen in the bottom of Figure 23 was created to assess the effect of the up-swept nose. Both configurations have the same wide-body and overall length, but the second geometry has a modified nose shape based on the nose shape of the Boeing 787. The modified nose is shorter than the D8 up-swept nose so the straight barrel section is extended forward to make up the difference in fuselage length. Note that the shapes of both noses were not aerodynamically optimized but shaped based on pilot visibility and equipment packaging considerations.

Since the metrics of interest are driven by inviscid effects, Euler calculations (inviscid, compressible) were conducted in Star-CCM+. Angle of attack sweeps were conducted at a freestream Mach number of 0.80, simulated altitude of 40 kft, and side slip angle of 0º. These conditions represent a potential cruise condition.

Figure 24 shows the resulting lift (left) and pitching moment (right) curves from the simulations of the two geometries. In addition to the total quantities of lift and pitching moment, the isolated contributions of the fuselage and wing are also shown. Focusing on the results for the nominal D8 nose, the fuselage contributes roughly 17.8% of the overall lift across the range of angles of attack. The fuselage carryover lift contribution found in this study is consistent with the quoted literature of 15-20% [8].

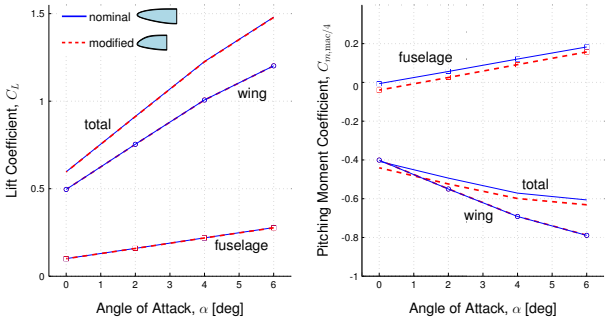

Fig. 24. Lift and moment curves from CFD for two fuselage options. Lift curves (left) and moment curves (right) for the CFD (Star-CCM+ Euler) fuselage nose study. Conditions: SSA 0°, M∞ 0.80, altitude 40 kft.

Analyzing the lift performance between the two geometries shows that the nose shape does not affect the magnitude of the carryover lift. There is a difference, however, between the two configurations' pitching moments. The modified nose shows a $\Delta C_{m,mac/4}$ = -0.03 which results in less of a restoring force on the airframe. Looking at the breakdown of the pitching moment contributions, the source of the pitching moment difference is unsurprisingly only from the fuselage. This finding is supported by the results from the low speed wind tunnel experiment which tested the two different nose shapes. These wind tunnel results are shown in Figure 25. It should be noted that the models tested in the wind tunnel test to assess the nose change had the D8 aft-end (i.e. Pi-tail and embedded nacelles) as well as a different wing geometry.

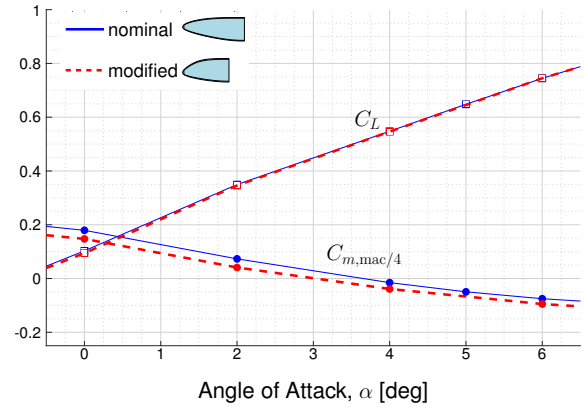

Fig. 25. Experimental data from 12-ft LST at NASA LaRC. Lift and moment curves comparing the two fuselage noses. Conditions: SSA 0°, M∞ 0.09, altitude sea-level.

5.4.2 Tail Configuration Aerodynamics

The D8's wide-body fuselage allowed for a Pi-tail empennage layout which provides mainly structural benefits. The main challenge for designing a Pi-tail at transonic speeds is managing the drag produced at the stabilizer intersections while still being able to meet structural requirements such as actuation device housing. The team performing this work has been actively exploring different Pi-tail designs, specifically taking inspiration from various T-tail aircraft to inform the blending of the stabilizer intersection.

Figure 26 shows an initial geometry for a Fokker 100-type Pi-tail design and Euler results for this geometry at cruise conditions. Unlike transonic T-tail aircraft, which has a strictly backward-swept horizontal tail, the Pi-tail has both forward- and backward sweeps relative to the stabilizer junction. As seen in the Euler results, there are regions of supersonic flow on the top surface of the inboard stabilizer junction, and the lower surface of the outboard horizontal tail. While forward-swept lifting surfaces are not terribly common in commercial aircraft, planes such as the Grumman X-29 have used this feature and were able to overcome this challenge. The over-speed on the outboard lower surface can be mitigated by more standard swept profile reshaping.

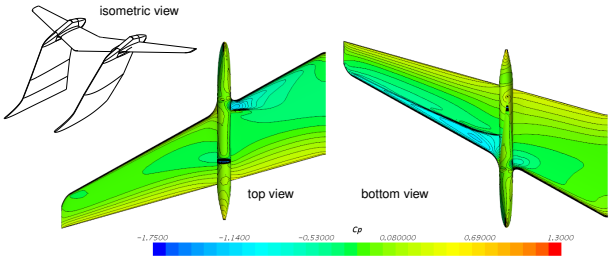

Fig. 26. Star-CCM+ Euler analysis of an early Pi-tail design. Left: Isometric view of the Pi-tail geometry. Middle: Top view of static pressure coefficient contours on the horizontal tail (vertical tail hidden). Right: Bottom view of static pressure coefficient contours on the horizontal tail (vertical tail hidden). Conditions: AoA 0°, SSA 0°, M∞ 0.78, alt. 35 kft.

Another challenge the Pi-tail design faces is the same challenge any T-tail variant faces which is the loss of stabilizer effectiveness during deep stall. As part of the low-speed configuration wind tunnel test, the Pi-tail layout was tested against a low-mounted horizontal tail (hereafter referred to as “low-tail”). While the low-tail may not be an efficient layout from a structural perspective, the low-tail would theoretically perform better in

deep stall. Both tail geometries can be seen on the right side of Figure 27. Both the low-tail and Pi-tail have the same tail span, but the Pi-tail has about 60% more exposed surface area and a 40% longer moment arm.

Figure 27 shows a comparison of the elevator effectiveness between the two tail layouts. Elevator effectiveness is defined here as the change in the model pitching moment about the m.a.c. quarter chord relative to the pitching moment at 0º elevator deflection. Positive deflections correspond to a downward elevator trailing edge. The Pi-tail configuration shows larger changes in pitching moment for the same amount of elevator deflection relative to the low-tail configuration. This is expected because the Pi-tail has additional inboard elevator. The elevator on the Pi-tail begins to lose its control authority around 15º angle of attack. The loss is more drastic as the deflection angle increases. The low-tail layout doesn't seem to experience much loss in control authority across the range of angles of attack, as expected. Information gained from this or any other future wind tunnel test will help inform the location of the horizontal tail as well as "keep-out" zones in the operating envelope.

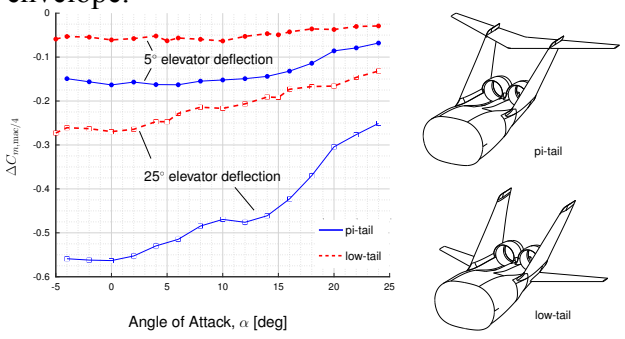

Fig. 27. Experimental analysis of tail configuration from 12-ft LST at NASA LaRC. Elevator effectiveness of the two tail layouts at 5◦ and 25◦ elevator deflection. Conditions: SSA 0◦, M∞ 0.09, altitude sea-level.

5.4.3 BLI Propulsion System Integration

The most intensive aspect of the D8 aerodynamic design is the integration of the propulsion system into the aft-fuselage and Pi-tail. Due to the complex nature of the geometry and flow regime (viscous, transonic), a majority of the design analysis was conducted using RANS CFD. A building-block approach to the conceptual design of the aft-end integration was used; the geometry was broken into its simplest components and then more geometric complexity was added in stages.

The primary aft-end design requirement at cruise is to minimize excess dissipation from the propulsion-fuselage integration, while still being able to diffuse the flow to the desired fan face Mach number. Analysis of preliminary aft-end geometries at cruise conditions identified two regions unique to the D8 configuration that could result in excess dissipation: (i) the space in between the nacelles and (ii) the junction between the nacelle and vertical tail.

The space in between the nacelles is highly susceptible to shocks because the inboard surfaces of the nacelles act like a convergent-divergent nozzle. Figure 28 (top) shows Mach contours on the symmetry plane at cruise conditions at an altitude of 35 kft and highlights the location of the shock. The aft-end body is translucently overlaid over the contours to give spatial context of the shock location. The highest Mach number seen in the channel has a value of 1.24. Recent work has determined that this shock can be mitigated by tailoring the local nacelle profile.

The nacelle-vertical tail junction is susceptible to flow separation, as the aft surfaces of the outer nacelle and vertical tail act as an effective diffuser, producing an adverse pressure gradient. In addition, high curvature near the nacelle lip can result in a weak shock-induced separation, exacerbated by the downstream diffusion. The wall shear stress traces in Figure 28 (bottom) show the extent of the shock-induced separation in an early aft-end design. Multiple steps were taken to address these flow features. The first was to tailor a patch surface between the outer nacelle and vertical tail toward the components' trailing edges. This patch surface adds volume to the body and subsequently reduces the level of flow diffusion. The second was to extend the leading edge of the outboard nacelle profile to blend smoothly into the vertical tail. This modification brings the local nacelle leading edge out (greater radius), reducing the curvature of the outer nacelle surface, and thus reducing the susceptibility to local shocks.

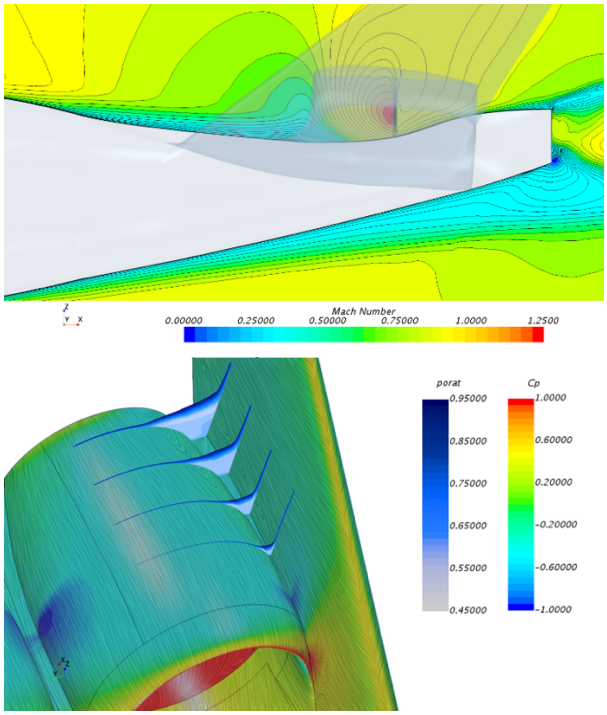

Fig. 28. Star-CCM+ RANS analysis on an early aft-end geometry highlighting unique D8 aerodynamic design challenges. Top: Mach contours on the symmetry plane with a translucent aft-end geometry overlaid. Bottom: Image of the vertical tail-nacelle junction. Surface contours show static pressure coefficient with traces of wall shear stress, and the off-body axial cuts show total pressure ratio; Conditions for both images: AoA 2◦, SSA 0°, M. 0.78, alt. 35 kft, FPR 1.5.

Detailed design of the aft-end is still in progress. The main conditions that drive the aero-design are cruise, start of descent, and take-off. Other conditions that require consideration are one-engine operation (engine out) as well as crosswind take-off. From a propulsor distortion standpoint, additional conditions of interest include ground-roll crosswind as well as very high angle of attack. At high angle of attack, there are some concerns that shed nose-vortices could be ingested into the propulsors. While this phenomenon did not appear in the low speed wind tunnel tests, it is something that needs to be evaluated at proper Reynolds and Mach numbers as part of a future work program.

5.4.4 Air Vehicle Drag Buildup

A table summarizing the profile drag areas is in Table 13. For comparison, published drag estimates [30] of a comparable sized aircraft, the Boeing 727-200, are shown. The latter airplane has a larger wing. Both aircraft have similar fuselage lengths; the total fuselage wetted area of OD8 is a bit larger because of the greater width, but that is compensated in part by less nacelle wetted area than the 727. The excrescence and unknown drag estimates for D8 are likely pessimistic, and as noted the tail is currently significantly oversized. Nevertheless, this comparison gives confidence in the validity of the drag buildup method, and assurance that it's not overly optimistic. Drag polars were developed using handbook methods for the fuselage and empennage, a vortex lattice method for the induced and trim drag, and an

	D8	Boeing 727-200		
		Method 1	Method 2	Method 3
Wings	7.643	8.665	8.940	9.607
Fuselage	8.638	8.432	8.700	8.700
Nacelles		1.074	1.896	2.007
Pylons	2.173	1.598	0.419	0.447
Centre Nacelle		2.188	2.323	2.525
Horizontal Tail	2.078	1.283	1.223	1.307
Vertical Tail	2.028	0.342	0.282	0.304
Flap Track Fairings	0.267	0.267	0.232	0.249
Total	22.827	23.849	24.015	25.146
Excrescences	2.985	2.673		1.752
Unknown	0.871	0.725		0.544
Total	26.683	27.247	26.309	27.442

Table 13. Subcritical profile drag with a comparison to three estimates for the Boeing 727-200.

Euler/integral boundary layer computational method for two-dimensional airfoil characteristics extended to three dimensions using simple sweep theory. High speed drag polars and the range factor, *M L/D,* are shown in Figure 29. The maximum lift-to-drag ratio at subcritical speeds is 19.1, with typical *L/D* of 17.4 at 0.78 Mach.

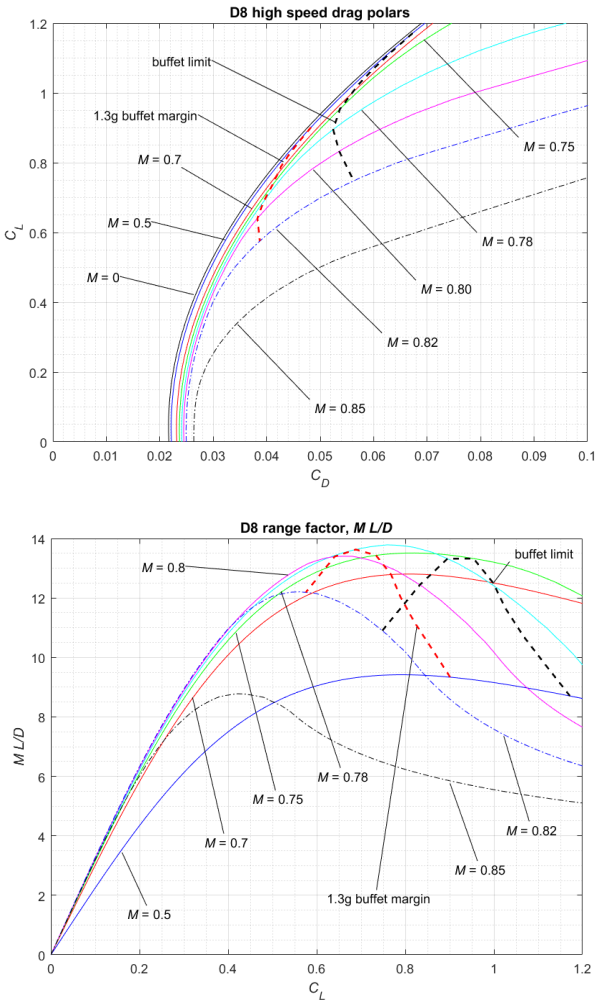

Fig. 29. High speed drag polars and the range factor *ML/D*

5.5 D8 Conceptual Design Summary

The performance of the 2016 D8 configuration described in the previous sections was evaluated using the tools described in Section IV. Based on the drag buildup, propulsion performance model, and the weight breakdown described above, the fuel consumption at the design payload-range was calculated using a forward-stepping Euler integration. An indicated airspeed limit of 250kts was used below 10,000ft, and flight path angles ranging from -2.0 to -3.0 were used during the descent phase of the mission. Based on this analysis, the block fuel burn benefit of the 2016 D8 is estimated to be approximately 25% better than a 737-800. The block fuel for the 737-800, 39,000lbs, was taken from the published airport planning guide. Block fuel for 3000 nm with a full passenger payload is 29,245 lb, or 18.5 passenger-nautical miles per pound.

5.6 System-Level D8 Benefit Assessment

A system-level analysis was conducted in order to assess the ability of the D8 aircraft to impact actual operational fuel consumption and reduce community noise impacts.

For the fuel assessment, flights originating or terminating in North America and serviced by American Airlines, Delta, JetBlue, Southwest, and United Airlines were simulated. The market demand is taken from 2014 OAG and the baseline aircraft performance is taken from Base of Aircraft Data (BADA 3). Baseline aircraft fleet composition for each airline is according to SEC reports and public statements. Aircraft growth and replacement is according to the 2016 Boeing Current Market Outlook, and fleet survival curves are based on H. Jiang [31]. New, non-D8 aircraft are assumed to improve by 1.5% per year. The Aurora D8-2016 presented in this paper is assumed to enter the fleet in 2025, with the TASOPT D8-2035 entering service in 2035. New D8 aircraft likewise improve at 1.5% per year. Note that these market entry dates are simply a point-of-departure for the system-level analysis.

Results are shown in Figure 30. Two aspects of this chart are notable; first, narrowbody aircraft currently contribute 55% of the baseline fleet fuel consumption. Therefore, designing an efficient aircraft for the narrowbody market is the biggest lever for impacting fuel consumption. Second, under the above assumptions, the D8 is able to save 52% of the projected narrobody fuel by in 2060, even when accounting for growth, replacement, aircraft survival rates, and baseline improvement.

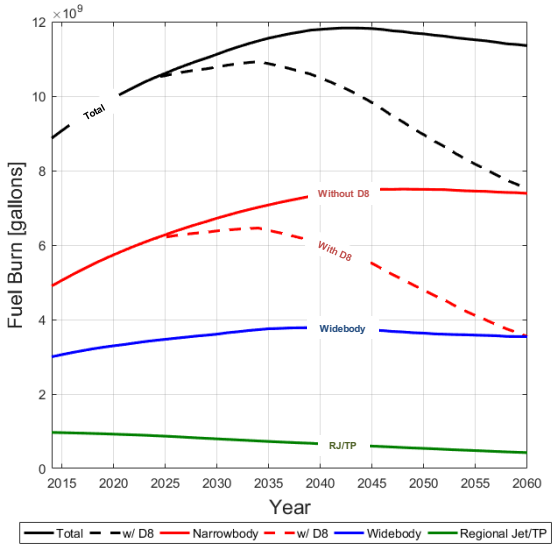

Fig. 30. System fuel forecast with and without the D8 (D8 only applied to the narrowbody market).

A noise assessment was also performed using a tool developed by L. Jensen, J. Hansman, et al. at MIT [32]. The tool links TASOPT with the NASA Aircraft Noise Prediction Program (ANOPP), and supplements this interaction with a flight profile generator. High-fidelity data from TASOPT, such as aircraft geometry, low-level engine parameters, etc., are passed to both a flight profile generator (to generate actual flight tracks) and to ANOPP in order to create noise grids. Those grids are then rotated and overlaid on specific airports of interests, and underlying population date from the 2010 census is used to calculate a change in population exposed on both a procedure level (Lmax) as well as on an integrated level (Day-Night Sound Level: DNL).

For integrated noise assessment, system-level operational data is taken from two sources. The data source for fleet operation count and fleet mix is the FAA Aviation System Performance Metrics (ASPM) Single Flight Download Records, with a range from 01 January 2015 – 31 December 2015. Runway configuration is based on ASPM Hourly Airport Efficiency reports, and operations are split proportionally between active runways in each one-hour window. Arrival and departure rates are calculated on an hourly, runway-specific basis for 2015; importantly, all operations are assumed to be straight-in arrivals or straight-out departures for simplicity and tractability. All flights utilize standard arrival and departure procedures: Instrument Landing System (ILS) 3° final for approach and ICAO1 Standard Departure profile. Baseline noise performance is using BADA for aircraft performance and the FAA Aviation Environmental Design Tool (AEDT) for noise modeling.

Results are shown in Figure 31. A sample approach (top left) at Los Angeles (LAX) is shown for the baseline aircraft, the 2016 D8, and the D8 with advanced technology. For this particular approach to runway 24R, 160,000 less people are exposed to 60dB L_{MAX}. In order to evaluate the integrated community noise impact, a year of operations were simulated at the top 20 airports by number of movements in 2015, as shown in Table 14.

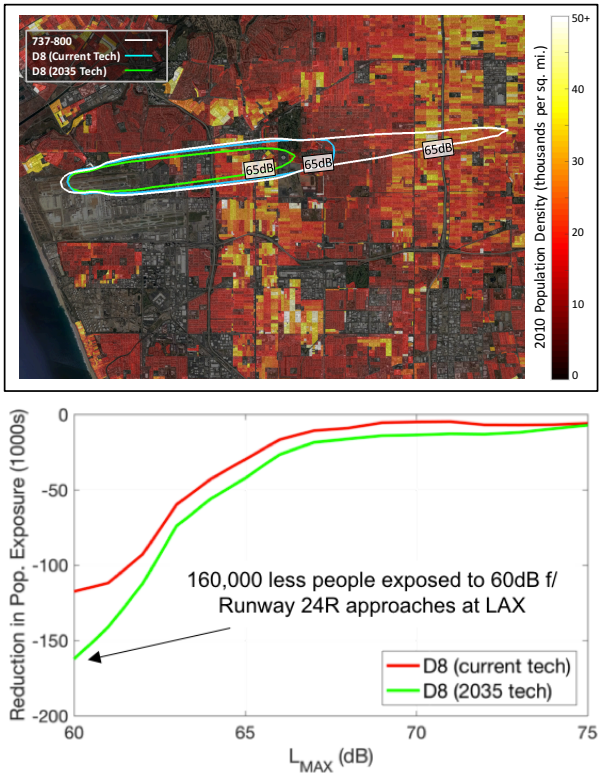

Fig 30. System-level noise assessment of the D8 aircraft. 65dB L_{MAX} approach noise contour for Los Angeles (LAX) runway 24R (top), reduction in population exposed for LAX runway 24R approach by dB level (bottom).

6 Conclusion

A conceptual design of a 0.78M, double-bubble, boundary-layer ingesting D8 aircraft was completed to provide higher fidelity estimates for weight and performance than recent studies using TASOPT. At the end of one full design cycle a viable 2016 D8 aircraft was achieved with an

Airport	Baseline (count)	D8 (Current Tech)	D8 (2035 Tech)	Reduction
ATL	81,005	49,736	39,826	41,179
ORD	152,594	72,423	56,275	96,319
DFW	41,960	5,881	4,125	37,835
LAX	263,190	143,960	126,749	136,441
DEN	88	25	9	79
CLT	12,513	4,771	2,483	10,030
IAH	17,180	7,451	5,714	11,466
JFK	409,659	307,259	270,355	139,304
SFO	10,288	3,270	2,921	7,367
PHX	39,841	21,279	11,213	28,628
EWR	88,304	58,712	53,775	34,529
PHL	30,395	16,524	13,483	16,912
MSP	50,722	22,361	17,427	33,295
SEA	92,170	42,425	33,812	58,358
DTW	9,661	1,472	751	8,910
LAS	138,327	56,527	40,826	97,501
LGA	259,663	100,049	67,524	192,139
BOS	68,652	22,674	18,544	50,108
MIA	160,756	102,769	90,367	70,389
MCO	17,614	3,584	1,063	16,551

Table 14. DNL population exposure reduction at top 20 busiest US airports. 60 dBA DNL; population from 2010 decennial census; 2015 yearly operations calculated on an hourly basis. D8 replaces narrowbody aircraft with similar capability. Reduction reported for 2035 variant.

MTOW = 153,670 lb. and a mission fuel for a 180 passenger, 3000 nm reference mission of 29,245 lb. This is a 25% block fuel improvement over the 737-800, and compares well with approximate 30% block fuel improvement predicted by TASOPT. There remain opportunities to further improve the efficiency of the aircraft designed in this paper – perhaps substantially – through further design cycles; those where they have been identified. At the same time as demonstrating much improved performance over current tube-and-wing configurations, the 2016 D8 was specifically designed to retain the ability to fit within the operational constraints and infrastructure of current airlines and airports.

As well demonstrating the fuel-efficient capabilities of the D8 configuration, this study led to a better understanding of the design challenges inherent in a new air-vehicle design, including the design and manufacturer of the double-bubble fuselage and empennage, the integration of the BLI propulsion system, and the overall air-vehicle design process and level of integration required between the airframe and engine manufacturer.

There is a clear need to continue development of the D8 concept, which is potentially a viable replacement for the current generation of single-aisle tube-and-wing aircraft. Further development is required to mature the concept, especially in regard to the BLI propulsion system, its integration with the airframe, and the details of the double-bubble fuselage design and manufacturer. These studies should be initiated in the near future. One potentially necessary risk reduction activity is thought to be the design and eventual manufacturer of a prototype aircraft, or X-Plane. A D8 X-Plane would demonstrate the D8 configuration performance and operability across the flight envelope, which is one of the largest remaining challenges associated with the configuration.

Acknowledgments

This work was sponsored by NASA, Contract #NND151C56C. Opinions, interpretations, conclusions, and recommendations are those of the authors and are not necessarily endorsed by the United States Government. The authors would like to acknowledge the management support of Brent Cobleigh, Rich DeLoof, and Mike Guminsky at NASA. The authors would also like to thank the talented team at Aurora Flight Sciences that have contributed to this work: Ian Bilyj, Matt Carstensen, Clinton Church, Stephen Clark, Andrew Coe, Patrick Cox, Paul Dahlstrand, Amanda Dropkins, Jeff Ensminger, Patrick Garrett, Jonas Gonzalez, Riley Griffin, Deborah Hoffman, Dr. Matthew Hutchison, Cody Jacobucci, Alex Kim, Dr. John Langford, Abraham Oonnoonny, Gary Papas, Alex Peraire, Vincent Posbic, Jason Ryan, Raymond Singh, Nina Siu, Jay Snider, Corey Stein, William Thalheimer, Josh Torgerson, Adam Treager, Nathan Varney, Ed Wen, and Travis Whitfield. The authors would especially like to thank Oliver Masefield for his invaluable technical contributions and commitment to the D8 team. Thanks also to the great researchers at MIT for

both their past and current contributions to making the D8 a reality, including but not limited to Professor Mark Drela, Professor Ed Greitzer, Professor John Hansman, Professor Warren Hoburg, Luke Jensen, Phillippe Kirschen, Berk Ozturk, Jacquie Thomas, and Martin York.

Lastly, the authors would like to thank the following individuals for their review and input during technical interchange meetings throughout the program: Scott Anders, Milind Birajdra, Richard Bradshaw, Mary Colby, Fay Collier, Dr. Alan Epstein, Starr Ginn, James Heidmann, Christopher Hughes, Nils Larson, Mary Jo Long-Davis, Wesley Lord, John Melton, Bruce Morin, Andrew Murphy, Zienna Nalles, Bradford Neal, Scott Ochs, Steve O'Flarity, Wally Orisamolu, Shishir Pandya, Gabriel Suciu, Neil Terwilliger, Dan Vicroy, Richard Wahls, Jason Welstead, et. al. Opinions, interpretations, conclusions, and recommendations in this paper are those of the authors and are not necessarily by the above individuals.

References

[1] Yutko B, Titchener N, Courtin C, Lieu M, Wirsing L, Tylko J, Chambers J, Roberts T, and Church C. Conceptual Design of a D8 Commercial Aircraft. *17th AIAA Aviation Technology, Integration, and Operations Conference, AIAA AVIATION Forum*, AIAA 2017-3590, 2017.

[2] Pamela M. "From Engineering Science to Big Science: The NACA and NASA Collier Trophy Research Project Winners," NASA SP-4219, 1998.

[3] Littlewood W. Technical Trends in Air Transport: The Sixteenth Wright Brothers Lecture. *J. Aeronaut. Sci.,* Vol. 20, No. 4, pp. 225-268, 1953.

[4] Christensen C. *Innovator's Dilemma: When new technologies cause great firms to fail.* 1997.

[5] Liebeck R. Design of the Blended Wing Body Subsonic Transport. *J. Aircraft.* Vol. 41, No. 1, pp. 10-25, 2004.

[6] Epstein A. Aeropropulsion for Commercial Aviation in the Twenty-First Century and Research Directions Needed. *AIAA J.* Vol. 52, No. 5, pp. 901-911, 2014.

[7] Greitzer E, et al. N+3 Aircraft Concept Designs and Trade Studies, Final Report Volume 1. NASA CR-2010-216794/VOL1, 2010.

[8] Drela M. Development of the D8 Transport Configuration. *29th AIAA Applied Aerodynamics Conference.* 2011.

[9] Follen G, Del Rosaria R, Wahls R, and Madavan N. NASA's Fundamental Aeronautics Subsonic Fixed Wing Project: Generation N+3 Technology Portfolio. 2011-01-2521, 2011.

[10] Blanco E and Hileman J. Noise Assessment of the Double-Bubble Aircraft Configuration. *49th AIAA Aerospace Sciences Meeting Including New Horizons Forum.* 2011.

[11] Pandya S, Huang A, Espitia A, and Uranga A. Computational Assessment of the Boundary Layer Ingesting Nacelle Design of the D8 Aircraft. *52nd Aerospace Science Meeting*. 2014.

[12] Hall D, Greitzer E, and Tan, C. Analysis of Fan Stage Conceptual Design Atttributes for Boundary Layer Ingestion. *J. Turbomach.* Vol. 139, No. 7, July 2017.

[13] Lord W, Suciu G, Hasel K, and Chandler J. Engine Architecture for High Efficiency at Small Core Size. *53rd Aerospace Sciences Meeting.* 2015.

[14] Uranga A, et al. Preliminary Experimental Assessment of the Boundary Layer Ingestion Benefit for the D8 Aircraft. *52nd Aerospace Sciences Meeting.* 2014.

[15] *FAA AC 120-27E – Aircraft Weight and Balance Control.* 2005.

[16] NASA Aeronautics Research Mission Directorate Strategic Implementation Plan: 2017 Update [Online]. Available: https://www.nasa.gov/aeroresearch/strategy [Accessed 30 May 2017]

[17] Boeing Commercial Airplanes. 737 Airplane Characteristics for Airport Planning.

[18] Bradley M and Droney C. Subsonic Ultra Green Aircraft Research. NASA CR-2011-216847, 2011.

[19] *FAA AC 25.773-1 – Pilot Compartment View Design Considerations.*

[20] *FAA NPRM Docket No. NM 185, Notice 25-01-02 -S C Special Conditions: Enhanced Vision System (EVS) for Gulfstream Model G-V Airplane.* 2001.

[21] Chambers J. Structural Optimization Study of the D8 Double-Bubble Composite Fuselage. *58th AIAA/ASCE/AHS/ASC Structures, Structural Dynamics, and Materials Conference,* 2017.

[22] *FAA AC 20-128A – Design Considerations for Minimizing Hazards caused by Uncontained Turbine Engine and Auxiliary Power Unit Rotor Failure Document Information,* 1997.

[23] *NASA G-7123.1-001 AFRC Aircraft Structural Safety of Flight Guidelines.*

[24] McCullers L. Flight Optimization System Release 8.23 User's Guide. 2011.

[25] Raymer D. *Aircraft Design: A Conceptual Approach.* Fourth Edition, 2006.

[26] Roskam J. *Airplane Design.* DAR Coproration, 2000.

[27] Darrieus G. La mécanique des fluids. Qulques progrès récents. *Conférence du 15.2.1938. La Technique Modern. Supplements des 15.9.1938, 1.8.1939 et 15.11.1941.*

[28] Kerrebrock J. *Aircraft Engines and Gas Turbines.* 1992.

[29] Vicroy D. Low-Speed Stability and Control Test of a Double-Bubble Transport Configuration. 2017.

[30] Obert E. *Aerodynamic Design of Transport Aircraft.* Amsterdam: IOS Press, 2009.

[31] Jiang H. Key Findings on Airplane Life. 2013.

[32] Jensen L, et al. Development of Rapid Fleet-Wide Environmental Assessment Capability. *AIAA AVIATION 2017*, 2017.

[33] Drela M. Power Balance in Aerodynamic Flows. *AIAA J.,* Vol. 47, No. 7, pp. 1761-1771, 2009.

Copyright Statement